HYDROGENOLYSIS OF POLYETHYLENE OVER EARTH-ABUNDANT COBALT CATALYSTS

A Thesis

by

SIDDHESH SHIRISH BORKAR

Submitted to the Graduate and Professional School of
Texas A&M University
in partial fulfillment of the requirements for the degree of

MASTER OF SCIENCE

Chair of Committee,	Manish Shetty
Committee Members,	Benjamin Wilhite
	Andy Thomas
Head of Department,	Victor Ugaz

May 2023

Major Subject: Chemical Engineering

ABSTRACT

In recent times, plastics have become indispensable to human life. The availability of raw materials, ease of production, and versatility have made plastics ubiquitous. The pollution, however, caused by improper disposal has become a major global concern. Most plastics used today are single-use and end up in landfills and water bodies. Only about 9% of them are recycled. To remedy plastic pollution's environmental consequences and move toward creating a circular plastic economy, effectively upcycling and recycling plastic waste has gathered significant attention. One avenue toward chemically repurposing polyolefins is via hydrogenolysis.

Hydrogenolysis is a depolymerization reaction wherein hydrogen molecules break the relatively inert C-C backbone of the polyolefin. Ru is regarded as the most active hydrogenolysis catalyst. This work studied the hydrogenolysis of polyethylene using earth-abundant cobalt immobilized on a neutral support, silica (Co/SiO_2). Co showed ~30% *n*-octadecane (*n*-C_{18}) conversion into the full range of C_1-C_{17} alkanes, compared to Ru (100% conversion to methane), Pt, Pd, and Fe (~3%, 0%, and 0% conversion, respectively). It was shown that Co/SiO_2 is an excellent catalyst that selectively converts polyethylene into liquid range hydrocarbons (C_5-C_{30}) at mild conditions (250-275 °C, 20-30 bar H_2, and 4-8 h). At optimized conditions (275 °C , 30 bar H_2, 8 h), ~19.5% gaseous and ~58.2% liquid products were yielded with an average liquid carbon of 22 (diesel-motor oil range). The catalyst further successfully converted end-of-use polyethylenes despite additives and impurities. The catalyst's active phase was CoO, and it showed exceptional regeneration between runs, giving nearly identical product distributions. Mechanistically, it was identified that Co favors the non-terminal C-C bond cleavage route, selectivity producing oligomers over gases at low conversions, which subsequently hydrogenolyze into lower hydrocarbons, eventually forming methane in secondary and tertiary events.

DEDICATION

To my parents, who are a constant source of inspiration

ACKNOWLEDGEMENTS

First and foremost, I thank my advisor Dr. Manish Shetty for making this research and thesis possible. He has been a pillar of support inside and outside the lab, and working under his mentorship has been a privilege. He offered me the opportunity to research an area I am passionate about, for which I am grateful. I learned something new daily and gained invaluable experience setting up the lab, writing papers, and asking and answering the tough scientific questions surrounding my project.

I want to extend my gratitude to my committee members, Dr. Benjamin Wilhite and Dr. Andy Thomas, for their support in preparing this thesis and their insightful thoughts, comments, and feedback on my work.

Next, I would like to thank all the members of my research group for their encouragement and direct and indirect contributions to my project. A special thank you goes to Ryan Helmer, whom I worked closely with on several aspects of the project.

I would also like to thank Ashley Henley and Terah Cooper for all their support and work behind the scenes in ensuring that every aspect of my program unfolded smoothly.

Finally, I would like to express my heartfelt gratitude toward my parents, family, and friends – here, in India, and those now spread across the world for their unconditional support and motivation throughout all the phases of my life. None of this would have been possible without you, and I am eternally grateful.

CONTRIBUTORS AND FUNDING SOURCES

Contributors

This work was supervised by a thesis committee consisting of Prof. Manish Shetty and Prof. Benjamin Wilhite of the Department of Chemical Engineering and Prof. Andy Thomas of the Department of Chemistry.

The calibrations and calculations associated with quantifying liquid and gas phase products in the results section were contributed mainly by Ryan Helmer (Department of Chemical Engineering), a graduate student in the research group. He further contributed by synthesizing several of the study's catalysts and helped develop the reaction workup procedure described in the experimental section.

Denis Johnson and Yinying Hua (Department of Chemical Engineering) did the X-ray diffraction analyses of the catalyst samples. Suraj Panicker (Department of Chemical Engineering) contributed to the reaction workups for a few reactions in the latter phases of the project.

All other work conducted for the thesis was completed by the student independently.

Funding Sources

A scholarship from the Artie McFerrin Department of Chemical Engineering, Texas A&M University, supported the graduate study.

This work was also made possible partly by funding from the Texas A&M Engineering Experiment Station (TEES) through a stipend for the role of Graduate Teaching Assistant at the Department of Chemical Engineering.

TABLE OF CONTENTS

LIST OF FIGURES

Page

LIST OF TABLES

Page

1. INTRODUCTION[1]

1.1 Plastics – Production, Disposal, Pollution, and Recycling

Plastics are integral to modern life and are ubiquitously found, from single-use polythene bags to life-saving biomedical devices.[1] Since Bakelite, the first synthetic polymer manufactured in the early 20th century, polymer production has grown exponentially, reaching ~400 MMt in 2017, and is projected to triple by 2050.[1-3] The ease of production and availability of raw materials from fossil sources. Low manufacturing costs have contributed to the "plastic boom" over the past few decades.[2] Monomer production accounts for ~7% of global oil and natural gas consumption and has been predicted to increase to 20% in 2050, in line with increasing demand.[4, 5] In the US, polymer production is estimated to consume 3,400 PJ (picojoules) of energy per year (~17% of the entire US manufacturing sector) and to emit 104 MMt CO_2 eq. of greenhouse gases (GHGs) annually.[6]

However, plastic production and consumption in these volumes have led to significant environmental concerns over the past few decades. Plastic wastes are responsible for widespread land, air, and water pollution. According to the United Nations, plastic pollution in oceans and water bodies will be doubled by 2030,[7] burgeoning into a daunting challenge for the current generation. Furthermore, the biodegradation of plastic takes between 20-500 years.[8, 9] **Figure 1** shows the current life cycle of plastic waste where 40% of plastics are landfilled, 35% leak into the environment, 16% are incinerated for energy recovery, and only less than 9% are recycled (~3 MMt out of 36 MMt of total plastics in 2018 in the US).[2, 3, 10,11]

[1] This section has been reprinted from Borkar, S. S., Helmer, R., Mahnaz, F., Majzoub, W., Mahmoud, W., Al-Rawashdeh, M., & Shetty, M. (2022). "Enabling resource circularity through thermo-catalytic and solvent-based conversion of waste plastics." Chem Catalysis **2**(12): 3320-3356.

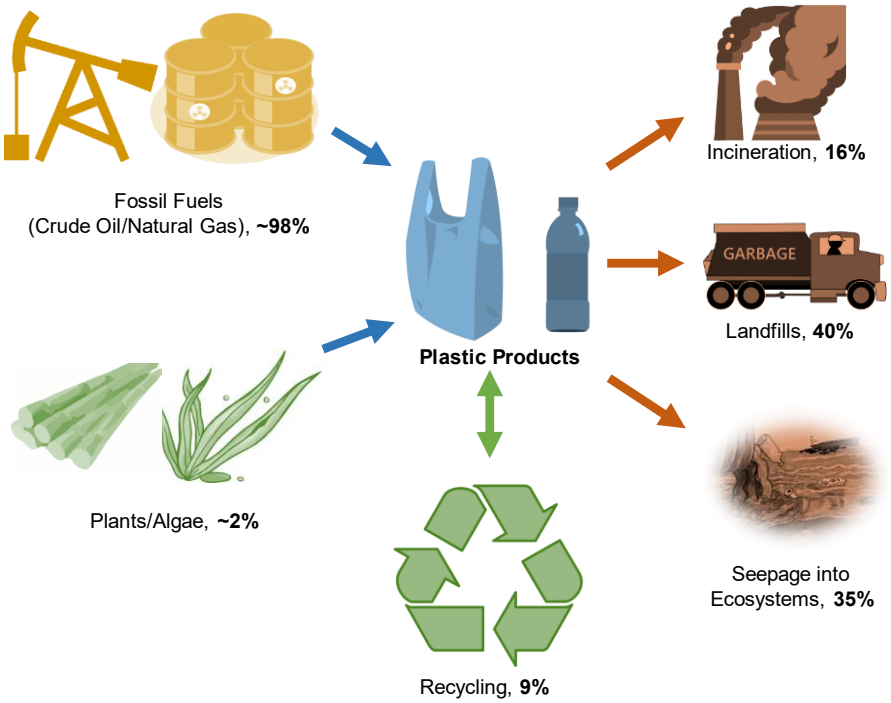

Figure 1. Linear plastics economy. Monomers are predominantly produced from fossil sources and a small fraction from plant/algae sources. After "end-of-use," plastics are either incinerated, discarded into landfills, seep into ecosystems, or recycled.

Estimates suggest that 75-199 MMt of plastic material currently exists, and 4.8–12.7 MMt/yr of plastic waste enters the oceans and assimilates into the marine environment, forming microplastics and disrupting aquatic life.[12] The inclusion of microplastics in the food chain threatens the health of our biosphere.[13] This is accompanied by releasing toxic compounds and metals into the surrounding ecosystems. Removing these oceanic plastics from accumulation zones using ships would need at least 50 years to make any significant impact. By then, the plastics would have been severely degraded to microplastics. Plastic pollution also poses health hazards for humans, including exposure to pathogens transported through plastic fragments across water bodies[14] and from inhaling toxic fumes and carcinogens from the unguarded incineration of

plastics.[15] To effectively mitigate the environmental release of plastics, a shift towards a 'circular economy' for plastics is essential.

Waste plastics represent a lost value of untapped carbon sources that could save up to 3.5 billion barrels of oil annually if utilized successfully.[5] Thus, the development of efficient technologies to tap these carbon sources can subside the plastics pollution problem two-fold; first, utilizing waste plastics will reduce the demand for fossil-based raw materials (inflow), and second, the release of plastic waste to the environment will drastically diminish compared to a linear plastics economy (outflow). **Figure 2** depicts the circularity of a plastics economy based on such methods.

While "primary" recycling entails the reuse of material for the same purpose, one of the prevalent methods of plastic waste recycling is *via* mechanical recycling ("secondary recycling" or material repurposing), which currently is used to recycle primarily PET and HDPE (29.1% and 29.3% of PET and HDPE, respectively, were recycled in 2018). However, this method often leads to the "downcycling" of plastics into lower-value products.[16] The heat and shear applied during mechanical recycling leads to chain branching, scission, and cross-linking of the molecules and degrade the mechanical properties. Contaminants such as pigments, dyes, and volatile components from processing lubricants also alter the polymers' chemical, mechanical, thermal, and rheological properties and lead to variability in the properties of the recyclate.[17]

Waste plastics are also incinerated ("quaternary" recycling) with municipal solid waste to harness their calorific value. Incineration destroys most plastic waste (solid content is reduced by 90%) and diverts it from landfills. However, it leads to substantial GHG and toxic emissions.[2, 18] Each ton of plastic waste contains approximately 79% carbon and, on incineration, would theoretically release up to 790 kg of carbon (~2.9 tons of CO_2) into the atmosphere.[19] In essence,

incineration leads to a loss of valuable carbon and promotes the continual use of fossil resources for plastic production, thereby making this process unfavorable for developing a true circular plastic economy (**Figure 2**).

On the path toward the circular economy of plastics, chemical repurposing ("tertiary" recycling) will play a critical role and needs extensive development. Within tertiary recycling, chemical recycling and upcycling comprise the principal two routes (**Figure 2**) to chemically convert "end-of-use" plastic materials to either precursor materials (monomers) to generate new plastics (*recycling*) or to "drop-in" replacements for fossil-derived fuels, lubricants, and waxes (*upcycling*).[20, 21] Chemical recycling targeted towards re-generating plastics herein is considered a "monomerization" process. While extraction of plastic monomers promotes an ideal, closed-loop cycle for the plastics economy, repurposing of wastes as replacements for fossil-based products (fuels, *etc.*) provides a unique opportunity for promoting "open-loop" pathways in the broader economy, fulfilling the idea of "recycling" in a general sense.[22] These options will prove pivotal in the gradual transition of the economy from linear to circular on the spectrum of resource circularity.

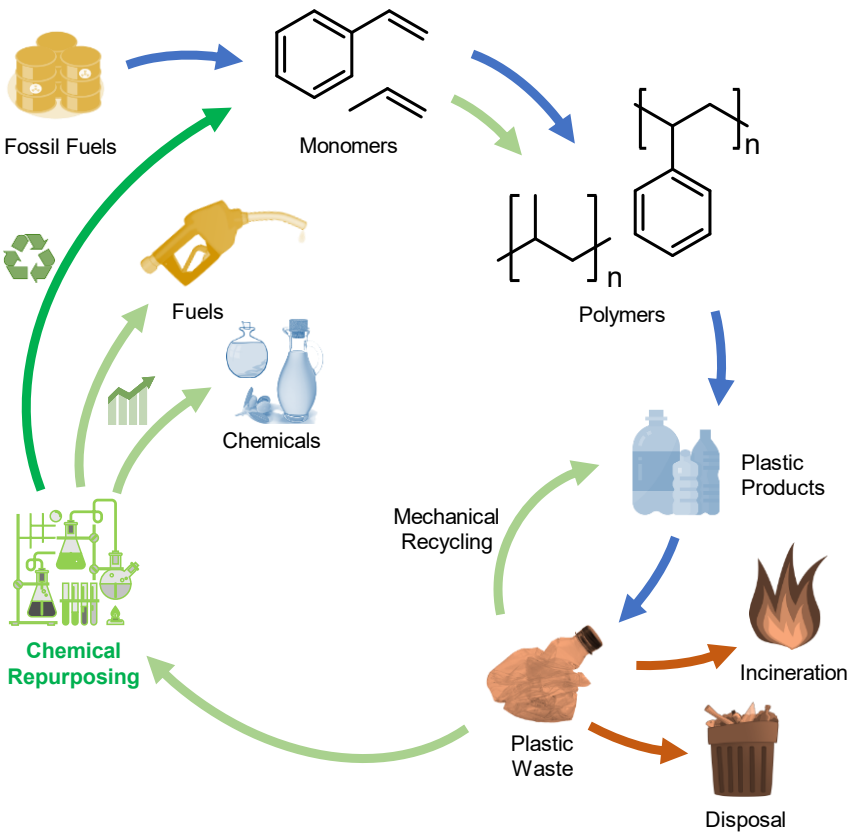

Figure 2. Circular economy of plastics. The blue arrows trace the current life cycle of plastics, from fossil sources to plastic products, and then discarded (dark orange arrows). The green arrows highlight the mechanical recycling and chemical repurposing strategies to recycle waste plastics in monomers (dark green), and upcycle them into various other chemical products, to enable the circular economy of plastics.

Several approaches have been explored in this regard, including hydrothermal liquefaction (HTL), gasification, pyrolysis, catalytic hydroconversion, and solvent-based depolymerization. HTL applies steam at high temperatures (300–550°C) and high pressure (250–300 bar) to convert the polymers into fuel oil.[13] Liquid yields above 90% have been reported using this method, preserving a large plastic fraction in the liquid phase.[13] Gasification, or partial oxidation, of polymers using air/steam is another route extensively studied in the literature.[4, 23] Its key benefits are the prevention of toxic byproduct formation and the production of *syngas* (carbon monoxide

and hydrogen) and hydrocarbons. The process typically involves an additional stage of Fischer-Tropsch synthesis to valorize *syngas*, which further requires significant energy inputs (temperature between 500-1300 °C) and syngas cleanup.[4, 23] Pyrolysis is also applied to decompose substrates using heat in an inert environment. This process has also been extensively studied and applied with commercial success.[24]

An alternative approach to creating a circular plastic economy is "intrinsically circular" plastics. These plastics, sourced from abundantly available hydrocarbon feedstocks, exhibit properties akin to conventional polyolefins while possessing the ability to be readily deconstructed back into their monomer compounds.[25] A recent perspective by Chen and coworkers provides detailed insight into the design principles of intrinsically circular polymers whose properties can be tailored.[26] These methods do not concern the repurposing of currently widespread plastic waste and instead propose a parallel, inherently circular plastic economy.

Plastics made from POs are the most abundant, and their products accounted for more than half of the total global plastics production in 2020, as shown in **Figure 3**.[27] POs are synthesized by the polymerization of olefins such as ethylene, propylene, styrene, *etc.*, and have repeating units connected by aliphatic C-C bonds.[2] Owing to their large production volumes, POs leak into ecosystems alarmingly.[3] Second in production to POs, condensation polymers are synthesized from the poly-condensation reactions between monomers by eliminating (typically) water molecules. Examples of condensation polymers include polycarbonates (PC) and polyamides (nylons), with polyesters being the most common. The condensation of alcohols and carboxylic acids synthesizes polyester. Among them, PET is the most abundantly produced polyester, with global production conservatively estimated at ~27.3 MMt in 2020 (although some sources estimate even higher amounts),[6] and is projected to rise to 32.8 MMt by 2030.[27]

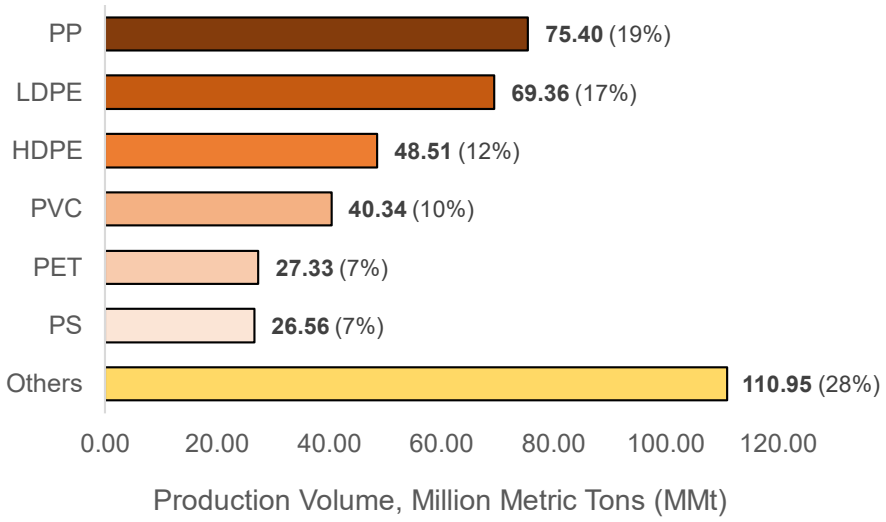

Figure 3. Global production volumes in million metric tons (MMt) of plastics (by type) in 2020.[27] The brackets represent the total production percentage.

1.2 Hydroconversion

Hydroconversion poses substantial promise in facilitating the chemical *upcycling* of polyolefins and polyesters, principally offering a means of converting wastes to valuable products. However, several reports also demonstrate chemical *recycling* to monomers, which is especially valuable regarding polyolefins resistant to solvent treatments. The hydroconversion reactions, which include hydrocracking and hydrogenolysis, involve cleavage of the C-C or C-heteroatom (C-O, C-N, *etc.*) bonds in a reacting substrate using H_2 gas.[17, 28] A hydrocracking catalyst is bifunctional, with metal and acid sites, whereas a hydrogenolysis catalyst has only metal sites.[28-30] Recent reports have used hydroconversion to deconstruct plastics into hydrocarbon molecules that can be used as fuels,[31] waxes,[32] and lubricants.[33] These reactions were (predominantly) carried out in a batch reactor with a supported metal catalyst in contact with melt-phase plastics under solvent-free conditions. H_2 pressure was varied between 1-50 bar at moderate temperature (150-350 °C) and varying contact times (1-48 h). This section will first discuss hydroconversion for

polyolefins, followed by polyesters. **Figure 4** shows the different catalysts, reaction conditions, conversion, and yield data reported for the hydroconversion of plastics.

1.2.1 Polyolefins

Many recent reports on plastic hydroconversion have focused on the most prevalent POs, as shown in **Figure 3**: PE (polyethylene) and PP (polypropylene). POs represent a significant fraction of the total landfilled plastic waste in the US. In 2019, 26,940 kt of PP and PE were landfilled, accounting for over 71% of plastic waste sent to landfills.[34] The estimated value lost through the disposal of PE and PP was between ~$2.9B and $8B, highlighting the importance of recycling these polymer types specifically for environmental and economic reasons. Therefore, among polyolefins, PE and PP are emphasized in this review. In the studies below, the main objectives were to maximize the valuable liquid products while minimizing the gaseous (*e.g.*, methane, ethane) and solid products, as shown in **Figure 4**. For instance, gaseous fuels like methane or natural gas have minimal market penetration in the transportation industry in the US compared to petroleum and liquid jet fuel.[35] While the combustion of plastic-based fuels still emits GHGs into the atmosphere, repurposing these wastes can reduce the overall dependency on fossil fuel resources and promote economic circularity in transitioning towards a closed-loop economy. To this end, the products listed in **Table 1** target liquid products due to their generally greater market applicability.

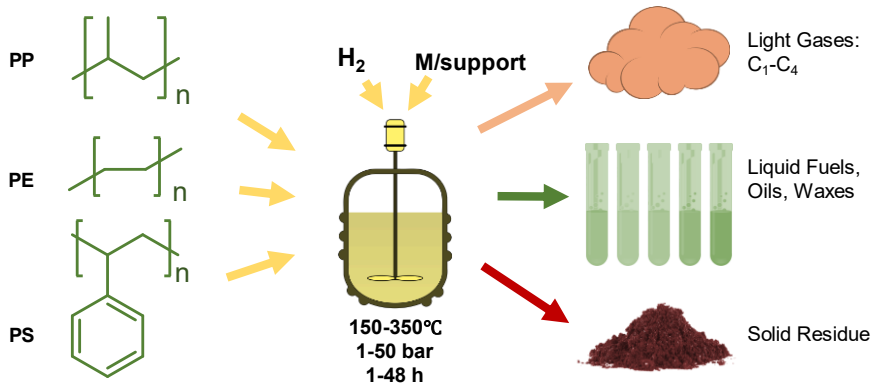

Figure 4. Typical polyolefin hydroconversion scheme. The polyolefins undergo hydrogenolysis in the melt phase in a batch reactor at 150-350 °C under 1-50 bar H_2 pressure and a contact time of 1–48 h. Supported metal or bifunctional metal-acid catalysts are typically utilized. The primary targets are the liquid hydrocarbons, including aromatics, fuels, lubricants, and waxes, with light gases and solid residues as side products.

Both the Pt group (Ru, Rh, Pd, Os, Ir, and Pt) and earth-abundant (Fe, Co, Ni, and Cu) metals have been used for the hydroconversion of waste plastics.[5, 36-39] Among these catalysts, Pt, Zr, and Ru were the most effective. *Ab initio* density functional theory (DFT) calculations reported that these metals have smaller energy barriers in model alkane C-C bond cleavage.[5, 40-42] In the following sections, the recent advances in the hydroconversion of plastics over supported Pt, Zr, and Ru catalysts are highlighted. Unless otherwise mentioned, all yield and conversion data is reported in mol%.

Platinum (Pt), a widely used hydrogenation and dehydrogenation catalyst,[43-47] has been keenly studied as a catalyst for PO hydrogenolysis. Celik et *al.* reported the transformation of PE into liquid products on Pt supported on $SrTiO_3$ ($Pt/SrTiO_3$) catalyst.[5] At 12 bar H_2 and 300°C for 96 h, the hydrogenolysis of PE (M_n, number-average molecular weight=8,150, PDI, polydispersity index=2.7) produced a lubricant-like product (M_n=590, PDI=1.1) with a 42% yield. Without any catalyst, the M_n only reduced from 8,150 to 5,700 while the PDI increased from 2.7 to 3.2,

suggesting that the catalyst played a crucial role in giving a narrow product distribution while also significantly reducing the molecular weight. $Pt/SrTiO_3$ also converted a wide variety of other PE samples (M_n=~15,000-160,000) to produce similar low M_n alkanes with a narrow dispersion (PDI=1.1-1.3). Surprisingly, the yield of alkanes increased from 42 wt % for the lightest PE to >99 wt % for the heaviest, suggesting that heavier PEs are more susceptible to hydrogenolysis (*vide infra*). Despite the presence of impurities, the complete conversion of an "end-of-use" plastic bag (M_n=33,000) into liquid products (M_n=990, PDI=1.3) was achieved.[5]

Bates and coworkers used an ultrawide-pore, silica-supported, bimetallic Pt-Re catalyst ($PtRe/SiO_2$) for the hydrogenolysis of perfectly linear HDPE, polystyrene (PS), linear low-density polyethylene (LLDPE), and poly(ethylene-alt-propylene) (PEP).[48] Kinetic analysis and DFT studies showed a C-C chain scission degradation mechanism associated with short butyl ($-C_4H_9$) branches at the tertiary carbon centers. Accordingly, at 170°C and 1 h, LLDPE degraded severely (M_W, weight-average molecular weight, reduced from 120,000 to under 11,000), while linear HDPE underwent the least chain degradation. Moreover, PS was completely hydrogenated to polycyclohexylethylene (PCHE) due to the absence of tertiary carbon centers.

To overcome the challenges of non-selective C-C bond cleavage on Pt catalysts, a catalytic architecture of mesoporous SiO_2 shells surrounding Pt nanoparticles, supported on a solid SiO_2 sphere ($mSiO_2/Pt/SiO_2$), was demonstrated to be effective for the hydrogenolysis of "end-of-use" high-density polyethylene (HDPE) and isotactic PP (i-PP) into a narrow distribution of liquid hydrocarbons by Tennakoon et *al.* and Wu et *al.*[49, 50] Specifically, hydrogenolysis of HDPE at 300°C and 8.9 bar H_2 for 15 h gave a narrow C_{23}-centered distribution of hydrocarbons. This result was consistent with the processive mechanism, akin to the enzyme-catalyzed processive deconstruction of macromolecules, where PE is suggested to be trapped in mesopores by polymer-

surface interactions causing terminal C-C bond cleavage on Pt sites and controlled release of smaller molecular-weight products with a narrow distribution. The mesopore architecture controls the chain scission. Thus, the resulting size of the hydrocarbon chains was tunable with the mesopore diameter. Furthermore, smaller-sized Pt nanoparticles (1.7 nm) were more reactive at similar reaction conditions than larger particles (2.9 or 5.0 nm).

Vlachos and coworkers have demonstrated hydrocracking on bifunctional Pt catalysts to selectively convert POs to branched liquid fuels (including diesel and gasoline-range hydrocarbons) with reduced gas yields. Mechanistically, the polymers undergo tandem catalysis with the activation of polymer over Pt sites first, followed by their cracking *via* β-scission and isomerization to branched hydrocarbons on acid sites, and concluded with the hydrogenation of olefin intermediates over metal sites (*vide infra*).[31] Accordingly, branched alkanes were produced with negligible gas yields from LDPE (M_w~76,000) using bifunctional Pt deposited on tungstated zirconia ($Pt/WO_3/ZrO_2$) at 250°C and 30 bar H_2 for 1-24 h. The metal-to-acid site molar ratio (MAB) (varied with the Pt and WO_3 content) substantially affected the product selectivity. By increasing the MAB ratio from 0.06 to 0.86, the ratio of C_{21+}/C_{4-6} increased from ~0.05 to ~0.7. It was hypothesized that at a high MAB ratio, olefins and paraffins establish pseudo-equilibrium with the metal sites. The slow acid-catalyzed reactions lead to deep isomerization before β-scission. At a low MAB ratio, isomerization and cracking occur through a parallel β-scission pathway that leads to a greater extent of C-C cleavage.[51]

A high yield (~60-85%) towards branched liquid fuels was demonstrated by Liu et *al.* at 250°C and 30 bar H_2 over a $Pt/WO_3/ZrO_2$ and HY zeolite mixture for several plastics, including LDPE (M_w= 250,000), i-PP (M_w= 250,000), HDPE, PS (M_w= 35,000), mixed layered plastics, bottles, and transparent bags (**Figure 5B**).[31] In another study, a bifunctional mechanism was

indicated by converting LDPE into liquid alkanes (C_5-C_{13}) at 63.6 wt % yield and an overall light alkane (C_1-C_{13}) yield of 94 wt % at 250°C and 30 bar H_2 for 1 h on Pt/WO_3/β-zeolite. The catalyst produced a narrow range of gasoline-grade alkanes from LLDPE, HDPE, and PP with liquid product yields as high as 74.5 wt % for HDPE.[52]

Utami et *al.* used Pt-promoted sulfated zirconia (Pt/SZr) to convert pyrolyzed LDPE into liquid hydrocarbons with a 74.60 wt % yield (0.15% solid and 25.25% gas) in a flow-reactor at 250°C and 1 bar H_2 for 1 h. The liquid product had 67.5 wt % of hydrocarbons in the gasoline range (C_5-C_{12}) and 7.1 wt % in the diesel range (C_{13}-C_{20}).[53] Furthermore, a higher catalyst acidity, controlled with Pt loading, was concomitant with higher yields of gasoline-range hydrocarbons (C_5-C_{12}).

A breakthrough in polymer synthesis was made by Ziegler and Natta in the 1950s when they discovered transition metal Ziegler-Natta catalysts for the polymerization of terminal olefins (α-olefins), ethylene, and propylene.[54] The Ziegler-Natta catalyst typically consists of transition metals with organometallic compounds, such as $Al(C_2H_5)_3$, as cocatalysts, immobilized on a support.[55] As the scale-up of this technology enabled the plastic boom, researchers began exploring catalysts for their depolymerization. Using the microscopic reversibility of Ziegler-Natta polymerization, transition metals akin to Ziegler-Natta catalysts were used to break down POs into lower aliphatic hydrocarbons.[56]

Basset and coworkers demonstrated the efficacy of a SiO_2-supported zirconium hydride, $(\equiv SiO)_3ZrH$, grafted by organometallic chemical reactions, to cleave C-C bonds under atmospheric pressure and mild temperatures (25-150°C).[57] Zirconium hydride catalyst with SiO_2-Al_2O_3 support was reported to convert PE and PP to lower alkanes (C_1-C_{17}) at low temperature (150°C) and 1 bar H_2. After 5 h, all the PEs (C_{20}-C_{50}, M_W=280–700) were converted to C_1-C_{17} products, and longer

reaction times (62 h) converted PE to lighter alkanes, eventually forming methane.[36] Heavier LDPE (M_W=125,000) showed 100% conversion to saturated oligomers at 150°C after 5-10 h. In addition, 40% of commercial i-PP (M_W=250,000) was converted into lower alkanes (C_1-C_7) at 190°C after 15 h.

An electrophilic (cationic) single-site organozirconium Zr-alkyl catalyst deposited on Brønsted-acidic sulfated alumina support, Zr[neopentyl]$_2$AlS, was shown to rapidly cleave C-C bonds in saturated hydrocarbons and a variety of plastics, namely, PE, i-PP, PE-co-1-octene (PECO), and a waste PE sandwich bag. Specifically, the supported Zr-H species produced C_1-C_{12} alkanes from *n*-hexadecane at 150°C and ~2.5 bar H_2 in 0.3 h. Under similar conditions (150-190°C and 2 bar H_2), an overall PE conversion of 95 wt % was observed after 2 h. PECO and i-PP both showed >96 wt % overall conversion after 1 h, whereas the PE sandwich bag took about 24 h to reach a comparable 96 wt % conversion.[42]

Ruthenium-metal catalysts have been reported to be the most active for the hydrogenolysis of various hydrocarbons.[33, 58] Notably, Almithn and Hibbitts reported through DFT calculations that the free-energy barrier for C-C bond cleavage of quasi-equilibrated dehydrogenated species from ethane (*CH-CH*) was the lowest for Ru among Group 8-11 transition metals for ethane hydrogenolysis.[40] Furthermore, Ru has been reported to be effective on both neutral (*e.g.*, Ru/C) and metal-oxide supports (*e.g.*, Ru/TiO_2, Ru/CeO_2) for PO hydrogenolysis.[32, 39, 59, 60]

Roman and coworkers focused on the catalytic hydrogenolysis of PE and PP to liquid alkanes.[39, 60] First, a series of metal and metal-oxide catalysts were investigated for the hydrogenolysis of *n*-octadecane (as a model PE), namely, Pt/γ-Al_2O_3, Ni/C, γ-Al_2O_3, NiO, Co_3O_4, RuO_2, Rh/C, Ru/Al_2O_3, and Ru/C under mild conditions (200-250 °C, 20-50 bar H_2) for 14 h. 5 wt % Ru/C was identified as the most suitable catalyst with 92 wt % conversion to produce *n*-

alkanes (C_6-C_{17}) and gaseous light alkanes (C_1-C_5) at high yields. For low molecular weight PE (M_w=4,000), 200 °C and 22 bar H_2 were optimum for producing liquid alkanes (C_8-C_{45}). A gradual shift in product distribution towards light gases (similar yields of methane, ethane, and propane at 200 °C; 3:1 ratio of methane to ethane at 225 °C; and pure methane at 250 °C) was observed as the reaction time was extended. The residue of solid products was also suppressed by increasing H_2 pressure from 15 bar to 20 bar, with any further H_2 pressure increase not leading to any variation in product distribution (**Figure 5A**).

To further demonstrate the efficacy of the catalyst, an LDPE (melt index 25 g/10 min) and a post-consumer LDPE bottle were converted by the Ru/C catalyst to liquid alkanes (C_8-C_{45}). Furthermore, two PP feedstocks (M_w=12,000 and 340,000) over the same catalyst under similar conditions produced liquid *iso*-alkanes (C_5-C_{42}). The former produced 68 wt % of liquid *iso*-alkanes at 225 °C and 20 bar H_2 over 16 h, while the latter required harsher conditions (225 °C and 50 bar H_2 over 24 h) to achieve a similar product distribution. Notably, the recycled catalyst showed minimal change in its activity for both PE and PP. A mixed substrate stream of PP and HDPE at 225 °C under 40 bar H_2 for 24 h produced a distribution of linear alkanes (C_5-C_{13}) and branched alkanes (C_7-C_{32}), enhancing their suitability in making diesel fuel blends.[61] Recently, Lin and coworkers demonstrated the effectiveness of the 5 wt % Ru/C in the presence of *n*-hexane as a solvent to produce maximum yields of 60.8 wt % and 31.6 wt % towards jet-fuel (C_8-C_{16}) and lubricant-range liquid hydrocarbons (C_{23}-C_{38}), respectively from HDPE plastic at 220 °C and 20-30 bar H_2. The maximum yield of liquid hydrocarbon products reached about 90 wt % within 1 h at 220 °C and 60 bar of H_2.[33]

Nakaji et *al.* employed LDPE (M_w=4,000) for screening metals on reducible CeO_2 support (M/CeO_2, M=Ru, Ir, Rh, Pt, Pd, Cu, Co, Ni) at 240 °C and 60 bar H_2 for 5 h.[32] Only Ru/CeO_2

showed an LDPE conversion of 76% at 5 h. The conversion increased to 99% at 8 h, with a total liquid yield of 90% (84% fuel and 7% wax) (**Figure 5C**). Ru on other metal-oxide supports (TiO_2, MgO, ZrO_2, SiO_2) and neutral carbon supports gave moderate conversions (66-83%) and liquid yields (39-73%). Importantly, Ru/CeO_2 was effective for converting LDPE (M_w=4,000-50,000), HDPE (M_w=64,000), PP (M_w=12,000), a plastic bag (M_w=177,000), and waste PEs at >99% conversions and yields for liquid fuels and waxes in the range of 83-91%.

A key disadvantage of Ru/C is the formation of light gases from POs, reducing liquid hydrocarbon yields. However, Ru/TiO_2 was shown to be a viable catalyst in converting PP to lubricants with high liquid yields under modest conditions.[59] Different samples of PP produced over 59 wt % liquid yields at 250 °C and 30 bar H_2 for 12-24 h over Ru/TiO_2, and the liquid products showed comparable physical properties to commercial lubricants. In contrast, Ru/C and Ru/CeO_2 formed light gases (C_1-C_6) under identical reaction conditions.

Ru supported on tungstated-zirconia (Ru-WZr) also significantly suppressed methane formation and produced diesel and wax/lubricant base oil (C_5-C_{35}) from LDPE (M_w=76,000) under mild conditions (250 °C, 50 bar H_2) and low reaction times (< 2 h) (**Figure 5D**). Crucially, this was unachievable on other acidic supports, such as Zr, WSi, HY zeolite, and mesoporous [Al]MCM-41.[62] The controlled hydrogenolysis was attributed to the capacity of $(WO_x)_n$ clusters to store H as surface hydroxyls by spillover, and this was hypothesized to be pivotal in the desorption of long alkyl intermediates that would otherwise undergo further C−C scission to produce methane. High liquid yields were also achieved on post-consumer LDPE bottles (73% liquid, 18% gas), cling wrap (67% liquid, 21% gaseous), and lab pipettes (40% liquid, 12% gas).[62] Interestingly, unlike bifunctional Pt catalysts, Ru on acidic supports showed no evidence of a bifunctional mechanism (*vide infra*). Hydrogenolysis using Ru-based catalysts has also been

reported to be effective on squalane, a C_{30} algae-derived branched hydrocarbon. This compound serves as a model to study the deconstruction of branched polymers. Tomishige and coworkers showed that Ru supported on C, SiO_2, and CeO_2 were promising catalysts for the hydrogenolysis of squalane to smaller hydrocarbons without isomerization and aromatization. Pt/C, Pd/C, Rh/C, and Ir/SiO_2 catalysts showed negligible reactivity at 240 °C and 35 bar H_2 pressure for *n*-hexadecane as a model substrate. In contrast, under identical conditions, Ru/C, Ru/SiO_2, and Ru/CeO_2 showed high reactivity (TOF, 79 h^{-1}, 180 h^{-1}, and 39 h^{-1}, respectively). Ru/CeO_2 was further used to hydrogenolyze squalane to a yield of 40% of either $C_{9\text{-}10}$ or $C_{14\text{-}16}$ products, depending on reaction time, demonstrating its capability of product selectivity.[63] The absence of light gases at low reaction times proved that the internal non-terminal H_2C-CH_2 bonds were preferentially cleaved over terminal C-C bonds. In another study, vanadium (V) was added to Ru to reduce the terminal C-C bond cleavage at longer reaction times. It was proposed that V species cover Ru particles and reduce the number of Ru ensembles active for terminal C-C cleavage. This effect was most remarkable on SiO_2 support. Ru-VO_x/SiO_2 (V/Ru = 0.25 mol) showed lower methane selectivity than Ru/SiO_2 and the highest $C_{14\text{-}16}$ selectivity among Ru/SiO_2, VO_x/SiO_2, VO_x/CeO_2, VO_x/MgO, VO_x/TiO_2, and VO_x/ZrO_2. PS was depolymerized into various arenes over Ru/Nb_2O_5 at 300 °C and 5 bar H_2 for 16 h.[64] The C-C bond of the sp^2-sp^3 bond connecting the aliphatic backbone to the phenyl groups was selectively cleaved to yield 76% of monocyclic arenes, despite the potential of hydrogenating the phenyl groups.[65] As such, PS was converted mainly into benzene (~50% yield) and ethylbenzene (~8% yield). Overall, supported Ru catalysts exhibited activity for hydrogenolysis of POs, even in the presence of acidic supports.

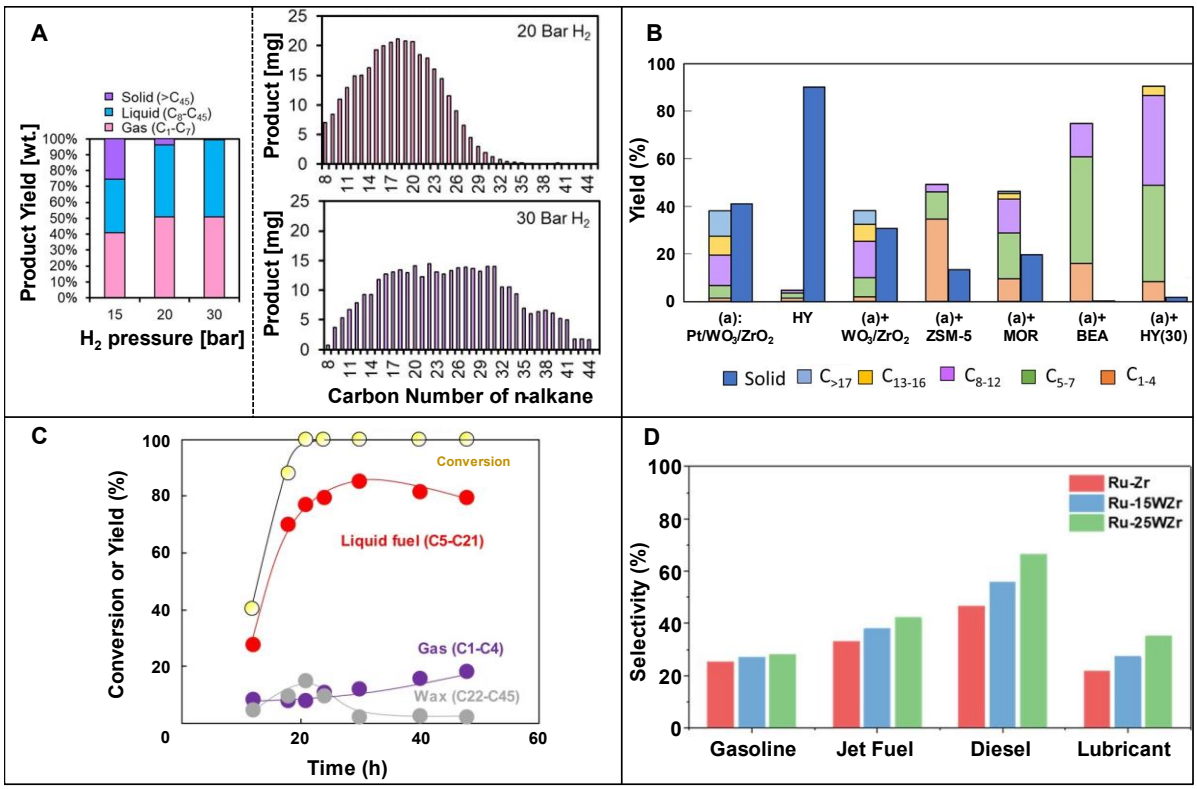

Figure 5. General trends in polyolefin hydroconversion. **A**. Solid, liquid, and gas product yields (Left) and corresponding liquid product distributions (Right) from hydrogenolysis of PE (M_w=4,000). Reaction conditions (Top-left): 100 mg PE, 25 mg 5 wt % Ru/C catalyst, 30 bar H_2, 16 h; (Other plots): 700 mg PE, 25 mg 5 wt % Ru/C catalyst, 200 °C, 16 h. Reprinted with permission from Rorrer et *al.*[39] Copyright 2020, The Authors. Published by American Chemical Society. **B**. effect of different supports on the product distribution in the hydrocracking of LDPE. Reaction conditions: 2 g LDPE, 0.2 g catalyst, 250 °C, 30 bar H_2, 2 h. Reprinted with permission from Liu et *al.*[31] Copyright 2021, The Authors. **C**. Product yields with reaction time in h from LDPE hydrogenolysis (M_w=4,000) over Ru/CeO_2 catalyst. Reaction conditions: 3.4 g PE, 500 mg 5 wt % Ru/CeO_2 catalyst, 200 °C, 20 bar H_2, 12-48 h. Reprinted with permission from Nakaji et *al.*[32] Copyright 2020, Elsevier. **D**. Effect on gasoline, jet fuel, diesel, and lubricant selectivity with varied WO_x loading in Ru-WZr catalysts on LDPE hydrogenolysis. (Top) Selectivities by fuel range: gasoline, C_5–C_{12}; jet fuel, C_8–C_{16}; diesel, C_9–C_{22}; and waxes/lubricant base-oils, C_{20}–C_{35}. Reaction conditions: 2 g LDPE, 50 mg catalyst, 250 °C, 50 bar H_2, 2 h. Reprinted with permission from Wang et *al.*[62] Copyright 2021, The Authors. Published by American Chemical Society.

1.2.2 Polyesters

PET can be chemically recycled via depolymerization into monomers, TPA, and EG and *upcycled* into other valuable chemicals.[66] The Milstein catalyst, a Ru coordination compound, is a versatile catalyst to synthesize esters and amides from the dehydrogenative coupling of alcohol and alcohol-amine pairs, respectively.[67] In contact with H_2 gas, the catalyst was activated for the reverse reaction, *i.e.*, hydrogenating esters to their corresponding alcohols.[68] Accordingly, milled PET from a used water bottle was hydrogenated into *p*-xylene glycol and EG at a conversion of above 99% in an anisole/THF solvent at 160 °C and 55 bar H_2 for 24 h.[69]

PET was also deconstructed to TPA and ethylene in a solvent-free hydrogenolysis pathway using a carbon-supported molybdenum-dioxo complex (MoO_2/C). The depolymerization was achieved at 1 bar H_2 pressure and 260 °C, with 87% yield to TPA.[38] Yan and coworkers performed catalytic hydroconversion of PET to arenes using a Co/TiO_2 catalyst. First, a pure TPA monomer was converted mainly to xylene and toluene with 75% and 9% yields at 340 °C and 30 bar H_2 pressure for 4 h (**Figure 6B**). Under similar conditions, PET formed xylene and toluene at 79% combined yield after 24 hr. However, a loss of catalytic activity was reported in the recyclability study due to Co leaching and the degradation of TiO_2 crystallinity.[37] Along with the hydrogenolysis of PS into benzene, Yan and coworkers demonstrated the use of Ru/Nb_2O_5 in converting several aromatic plastics (PET, PS, poly(p-phenylene oxide) (PPO), and PC) into arene monomers. For PET alone, the catalyst yielded 95.2% C_6-C_8 products. When applied to an equal mixture of PET, PS, PPO, and PC, the catalyst yielded 78.9% C_6-C_{10} arene products. Direct conversion of a PET waste bottle produced 90.9% C_6-C_8 yield (78.4% arenes) at 200 °C and 3 bar H_2 pressure for 8 h (**Figure 6A**). In contrast, Pd and Pt on Nb_2O_5 support produced cycloalkanes due to secondary hydrogenation of the arenes.[64]

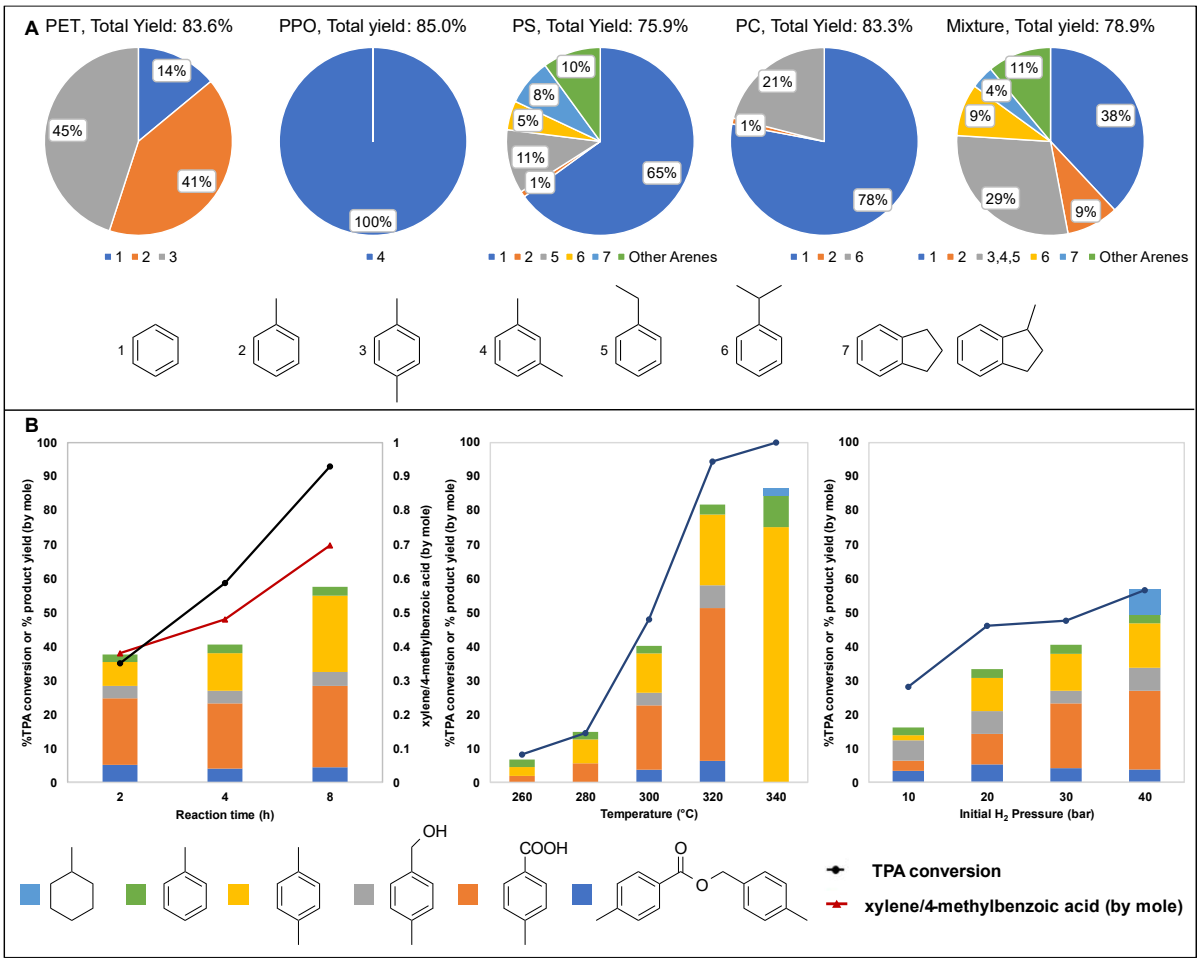

Figure 6. General trends from polyester hydroconversion. **A**. Product distributions from hydrogenolysis of aromatic plastics over Ru/Nb_2O_5. Reaction conditions: 30 mg feed, 30 mg Ru/Nb_2O_5 catalyst, 4 g octane, 5 bar H_2. PET: 280 °C, 8 h; PPO: 280 °C, 16 h; PS: 300 °C, 16 h; PC: 320 °C, 16 h; Mixed Feed: 15 mg PET, 15 mg PC, 15 mg PS, 15 mg PPO, 60 mg Ru/Nb_2O_5 catalyst, 4 g octane, 320 °C, 5 bar H_2, 16 h. Adapted with permission from Jing et *al.*[64] Copyright 2020, Wiley-VCH GmbH. **B**. effect of reaction parameters on TPA conversion and product yields obtained from hydrodeoxygenation of TPA over Co/TiO_2 catalyst: (Left) reaction time, (Centre) reaction temperature, and (Right) initial H_2 pressure. Reaction condition: 30 bar initial H_2, 300 °C, 4 h. Adapted with permission from Hongkailers et *al.*[37] Copyright 2021, Wiley-VCH GmbH.

Poly(butylene succinate) (PBS) is a bio-degradable polyester that degrades to CO_2 and water between 6-10 months at 25-50 °C. Pyrolysis of PBS was reported to produce a mixture of succinic acid, succinic anhydride, and tetrahydrofuran (THF), albeit at high temperatures above 400 °C.[70] In search of milder reaction conditions, catalytic hydrogenolysis over Pd/C was used to selectively produce THF at 240 °C and 60 bar H_2, at 53-60 wt % yield after 12-36 h.[71]

The hydroconversion of polyesters formed monomers and chemical precursors, including aromatics that can recycle plastics or form "drop-in" replacements for otherwise fossil-derived chemical precursors. **Table 1** below provides a comparative overview of hydroconversion catalysts and the influence of crucial reaction parameters such as catalyst loading, reaction temperature/pressure, and substrate type on the yield and selectivity of upcycled liquid products.

In sum, supported Pt, Zr, and Ru are active hydroconversion catalysts to chemically *upcycle* POs to liquid commodities with significant market potential, particularly transportation fuels, waxes, and lubricants. While Ru and Pt-based catalysts have shown considerable promise in producing liquid-range hydrocarbons that can serve as drop-in replacements for fuels and lubricants, reducing our dependence on virgin fossil sources, their deployment on a mass-scale is hampered by scarcity and costs associated with mining and processing.[72, 73] Alternate, earth-abundant metal-based catalysts are thus in great demand to enhance the broader applicability of hydrogenolysis. Cobalt and nickel are promising candidates that have not yet been explored greatly. Nickel has recently been studied in deconstructing LDPE substrates to n-alkanes, with insight also being provided on the possible mechanistic pathways over the catalyst.[74] Cobalt was reported to selectively produce propane over a Co/ZSM-5 catalyst.[75] While these studies have recognized the promise of earth-abundant metals as alternatives to the noble metal hydrogenolysis catalysts, a deeper mechanistic understanding is needed to leverage the specific properties of these

elements to design catalysts to selectively produce desired hydrocarbons. In this work, cobalt on silica (Co/SiO_2) has been studied in selectively converting polyethylene substrates into liquid hydrocarbons (C_5-C_{30}) at mild conditions (275 °C, 4-8 h, and 30 bar H_2). **Figure 7** shows a schematic overview of this reaction, with average liquid phase carbon numbers typically between 20 and 25 and low branching (<5%). The study has shown the catalyst's preference for non-terminal C-C bond cleavage over terminal C-C bond cleavage and excellent reusability, thus establishing cobalt as a viable active metal for polyolefin hydrogenolysis.

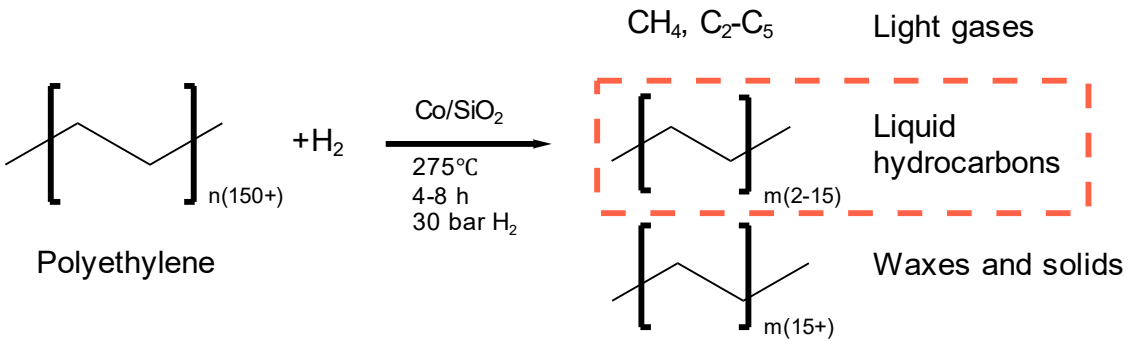

Figure 7. Hydrogenolysis of polyethylene substrates over Co catalysts at mild conditions.

Table 1. Summary of recent works on the hydroconversion of polyolefins and polyesters. The table highlights the substrate/polyolefins, catalyst and reaction parameters, and nature and quantitation of product yields.

Substrate	Catalyst	Catalyst Metal Loading (wt%)	Catalyst /Feed Ratio (wt)	Temp (°C)	Pressure (bar)	Time (h)	Product(s) of Interest	Product C_N	Product Yield (mol%)	Ref.
PE (M_w=22000)	$Pt/SrTiO_3$	11.10%	0.200	300	12	96	Waxes and lubricants	C_{42}[a]	42%[b]	5
PE (M_w=17000)				300	12	96		C_{47}[a]	68%[b]	
PE (M_w=70000)				300	12	96		C_{57}[a]	91%[b]	
PE (M_w=420000)				300	12	96		C_{59}[a]	>99%[b]	
Plastic bag				300	12	96		C_{70}[a]	97%[b]	
PE (M_w=3500)	$Pt/\gamma\text{-}Al_2O_3$	1.50%	1.667	280	N/A	24	Alkylaromatic Liquids; Waxes	C_{30}[a]	75%[b]	10
PE (M_w=3500)				280	N/A	24		C_{34}; C_{39}[a]	70% (46%; 24%)[b]	
LDPE bag				280	N/A	24		C_{27}; C_{26}[a]	69% (39%; 30%)[b]	
HDPE bottle cap				280	N/A	24		C_{20}; C_{35}[a]	55% (20%; 35%)[b]	
LLDPE	$PtRe/SiO_2$	[c]	1.000	170	35 (D_2)	17	Lower *n*-alkanes (M_w~6000)	C_{179}[a]	[c]	48
HDPE				170	35 (D_2)	17	Lower *n*-alkanes (M_w~98000)	C_{1666}[a]	[c]	
PEP				170	35 (D_2)	17	Lower PEP (M_w~74000)	C_{4400}[a]	[c]	
PS				170	35 (D_2)	17	PCHE (M_w~88000)	C_{6100}[a]	[c]	

Table 1 continued

Substrate	Catalyst	Catalyst Metal Loading (wt%)	Catalyst /Feed Ratio (wt)	Temp (°C)	Pressure (bar)	Time (h)	Product(s) of Interest	Product C_N	Product Yield (mol%)	Ref.
PE (M_w=90000)	$mSiO_2/Pt/SiO_2$	0.085% (1.7 nm)	0.0085	300	8.9	15	Wax	C_8-C_{36}	74%[b]	49, 50
i-PP				300	8.9	12			73%[b]	
LDPE	$Pt/WO_3/ZrO_2$	0.5% Pt; 15% WO_3	0.100	250	30	12	Fuels and Lubricants	C_4-C_{30} (C_7-C_{12})	>99% (65.2%)	51
LDPE	$Pt/WO_3/ZrO_2$ + HY(30) (Phys. mixture)	0.5% Pt; 15% WO_3	0.100	250	30	2	Liquid fuels (Gasoline, diesel)	C_5-C_{22} (C_5-C_{12}, C_8-C_{22})	82% (78%, 42%)	31
i-PP				250	30	2			82% (74%, 53%)	
i-PP/LDPE/PS				250	30	4			68% (63%, 41%)	
LDPE	$Pt/WO_3/Beta$	2% Pt; 0.5% W	0.025	250	30	1	Light Gasoline	C_5-C_{13}	63.60%[b]	52
LLDPE				250	30	1			65.00%[b]	
HDPE				250	30	1			74.50%[b]	
PP				250	30	1			52.30%[b]	
LDPE	$Pt/SZrO_2$	1.50%	0.010	250	1 bar; 20mL/min	1	Liquid fuels	C_5-C_{20} (C_5-C_{12}, C_{13}-C_{20})	74.60% (67.5%, 7.1%)[b]	53
PE (HMW)	$ZrH(SiO)_3$	3%	0.000	150	1	5	Oligomers	C_{10}-C_{17}	100%	36
i-PP				190	1	15	Light gases	C_1-C_7	40%	
PE	$ZrNp_2/SAl_2O_3$	1.4% Zr	0.150	150	2	0.83	*n*-alkanes	C_{10}-C_{26}	43%[b]	42
i-PP				190	2	1	branched-alkanes	C_{10}-C_{30}	68%	
PECO				190	2	1	*n*-alkanes	C_{12}-C_{22}	15%[b]	

Table 1 continued

Substrate	Catalyst	Catalyst Metal Loading (wt%)	Catalyst /Feed Ratio (wt)	Temp (°C)	Pressure (bar)	Time (h)	Product(s) of Interest	Product C_N	Product Yield (mol%)	Ref.
PE (model)	5% Ru/C	5%	0.040	200	22	14	*n*-alkanes	C_8-C_{45}	45%[b]	39
PE (LLDPE)			0.050	225	22	16	*n*-alkanes	C_8-C_{20}	53%[b]	
LDPE			0.036	225	22	16	*n*-alkanes, branched alkanes	C_8-C_{45}	48%[b]	
LDPE Bottle			0.125	225	22	2	*n*-alkanes, branched alkanes	C_8-C_{45}	48%[b]	
i-PP (LMW)	5% Ru/C	5%	0.143	225	20	16	iso-alkanes	C_8-C_{42}	68%[b]	60
i-PP (HMW)			0.071	250	40	8		C_5-C_{32}	35%[b]	
i-PP (HMW)			0.071	225	50	24		C_5-C_{32}	39%[b]	
HDPE/i-PP			0.036	225	40	24	*n*-alkanes, branched-alkanes	C_5-C_{32}	25%[b]	
HDPE	5% Ru/C	5%	0.500	220	30	1	Jet fuels; diesel fuels	C_8-C_{38} (C_8-C_{16}, C_{17}-C_{22})	75% (61%, 14%)[b]	33
HDPE			0.500	220	60	1	Jet fuels; lubricant hydrocarbons	C_8-C_{38} (C_8-C_{16}, C_{23}-C_{38})	87% (38%, 18%)[b]	
LDPE	Ru/CeO_2	5%	0.029	240	60	8	Liquid Fuels, Wax	C_5-C_{45} (C_5-C_{21}, C_{22}-C_{45})	90% (84%, 7%)	32
LDPE				240	60	18			88% (82%, 5%)	
LDPE				240	60	24			87% (80%, 7%)	
HDPE				240	60	10			87% (83%, 4%)	

Table 1 continued

Substrate	Catalyst	Catalyst Metal Loading (wt%)	Catalyst /Feed Ratio (wt)	Temp (°C)	Pressure (bar)	Time (h)	Product(s) of Interest	Product C_N	Product Yield (mol%)	Ref.
PP	Ru/CeO_2	5%	0.059	240	60	72	Liquid Fuels, Wax	C_5-C_{45} (C_5-C_{21}, C_{22}-C_{45})	83% (72%, 10%)	32
Plastic Bag/LDPE			0.147	200	20	30			91% (87%, 4%)	
Waste PE/ LDPE				200	20	48			88% (87%, 2%)	
i-PP (HMW)	Ru/TiO_2	5.90%	0.050	250	30	16	Oil	C_{49} avg, C_7-C_{200}[a]	66%[b]	59
i-PP (HMW)			0.025	250	30	24		C_{87} avg, C_7-C_{760}[a]	73%[b]	
i-PP (LMW)				250	30	12		C_{122}[a]	80%[b]	
a-PP				250	30	16		C_{159}[a]	71%[b]	
PP bag				250	30	16		C_{105}[a]	68%[b]	
PP bottle				250	30	20		C_{164}[a]	59%[b]	
LDPE	$Ru\text{-}15WZrO_2$	5%	0.025	250	50	2	Fuels and Lubricants, normal & branched	C_5-C_{35}	60%	62
LDPE Bottle				250	50	2			73%	
LDPE Cling Wrap				250	50	1.5			67%	
LDPE Pipette				250	50	1.25			40%	
n-hexadecane	Ru/CeO_2	5%	0.044	240	60	1	Gases, Light Liquids	C_1-C_{15}	19%	63

Table 1 continued

Substrate	Catalyst	Catalyst Metal Loading (wt%)	Catalyst /Feed Ratio (wt)	Temp (°C)	Pressure (bar)	Time (h)	Product(s) of Interest	Product C_N	Product Yield (mol%)	Ref.
Squalane			0.024	240	60	6	Specific liquid hydrocarbons	C_9-C_{26}	60%	63
Squalane	Ru/TiO_2	5% Ru	0.024	240	60	12	Liquid alkanes	C_9-C_{30}	76%	76
Squalane	$Ru\text{-}VO_x/SiO_2$	5% Ru; 0.63% V	0.071	240	60	15		C_9-C_{30}	46%	
Squalane			0.024	240	60	96		C_9-C_{19}	64%	
n-hexadecane			0.009	240	60	2		C_9-C_{15}	4%	
PET	Ru/Nb_2O_5	2%	1.000	200	3	12	Aromatics, Cycloalkanes	C_6-C_8	95%	64
PET				280	5	8	Aromatics (BTX, EB, Cumene, etc.)	C_6-C_{10}	84%	
PPO				280	5	16			85%	
PS				300	5	16			76%	
PC				320	5	16			83%	
PET/PPO/PS/PC				320	5	16			79%	
Polyester (model)	Milstein catalyst #2	-	0.028	120	13.8	24	1,10 decane diol	C_{10}	80%	69
PET (bottle)	Milstein catalyst #4		0.050	160	55.1	24	Ethylene glycol, p- Xylene glycol	C_2, C_8	>99%	
PLA (cup)	Milstein catalyst #4		0.133	160	55.1	24	Propylene glycol	C_3	>99%	
PPC	Milstein catalyst #2 or 4		0.048	160	55.1	24	Propylene glycol, methanol	C_1, C_3	>99%	
PEC	Milstein catalyst #2 or 4		0.026	160	55.1	24	Ethylene glycol, methanol	C_1, C_2	91%	
PHB	Milstein catalyst #4		0.050	160	55.1	24	Butyric acid	C_4	88%	

Table 1 continued

Substrate	Catalyst	Catalyst Metal Loading (wt%)	Catalyst /Feed Ratio (wt)	Temp (°C)	Pressure (bar)	Time (h)	Product(s) of Interest	Product C_N	Product Yield (mol%)	Ref.
P3HP	Milstein catalyst #4		0.130	160	55.1	24	Propionic acid	C_3	90%	69
PET (powder)	MoO_2/C	3.23% Mo	0.760	260	1	24	Terephthalic acid	C_8	87%	38
PET (bottle)			0.875	260	1	24			86%	
PET (TPA as model)	Co/TiO_2	5%	[c]	340	30	4	Arenes (Xylene, Toluene)		84%	37
PET (TPA as model)				320	30	4	Arenes (Xylene, Toluene, p-Toluic acid, etc.)	C_7- C_{16}	82%	
PET				320	30	8	Arenes (Xylene, Toluene, Cumene)	C_7-C_{20}	57%	
PET				320	30	24		C_7-C_9	79%	
PBS	Pd/C	5%	0.100	240	60	36	Liquids (incl. THF)	C_4-C_8	79.4% (59.5% THF) [b]	71
PBS				240	60	12			86.3% (35.8% THF) [b]	

Notes: Distinct products (and their corresponding carbon numbers and yields) are separated by ";" as reported in their respective studies, whereas those separated by "," have been reported as a single product class, PEC: polyethylene carbonate, PHB: poly(R-3-hydroxybutyric acid), PHP: poly(3-hydroxypropionic acid), PPO: poly(p-phenylene oxide). [a]CN calculated from article data (M_n/14). [b]Mass (wt %) yield. [c]Data not reported.

2. EXPERIMENTAL[2]

2.1 Materials

Cobalt(II) nitrate hexahydrate (ACS reagent, 98%, Sigma-Aldrich), iron(II) nitrate nonahydrate (ACS reagent, 98%, Sigma-Aldrich), ruthenium (III) nitrosyl nitrate in dilute nitric acid (Sigma-Aldrich), palladium (II) nitrate dihydrate (40% Pd basis, Sigma-Aldrich), tetraamine platinum(II) nitrate (99.995%, Sigma-Aldrich), and nickel(II) nitrate hexahydrate (99.995%, Bean Town Chemical) precursors were used to synthesize the supported catalysts.

The support, silica (fumed), was purchased from Sigma-Aldrich. Pentane (reagent grade, Ward's Science) and hexane (ReagentPlus, 99%, Sigma-Aldrich) were used for GC product identifications, and octadecane (99%, Sigma-Aldrich) was used for liquid phase product calibration and as a model compound. Benzene (HPLC grade, 99.9%, Sigma Aldrich) was used as the internal liquid phase product calibration standard. Ethyl acetate (ACS grade, 99.5%, VWR) was used as a solvent for liquid product extraction.

Polyethylene (average Mw ~ 4,000 g/mol, Sigma-Aldrich) was used as the primary substrate in the study, while HDPE (VWR solvent jug), LDPE (packaging bag and VWR solvent bottle), and PP (fruit cups) were directly used after cutting them into ~3-4 mm square pieces. All commercially obtained chemicals were used without further purification.

[2] This section is from a manuscript in-preparation. Borkar, S. S., Helmer, R., & Shetty, M. (2023). "Reactivity Investigation and Mechanistic Insights for the Hydrogenolysis of Polyethylene over Silica-supported Earth-abundant Cobalt Catalysts" ACS Sustainable Chemistry & Engineering.

2.2 Catalyst Synthesis

Catalysts were prepared by the incipient wetness impregnation method. In brief, first, distilled water was used to make aqueous solutions of the metal precursors at room temperature. Next, an appropriate amount of support was weighed in a beaker, and the precursor solution was added dropwise to the support, followed by vigorous stirring using a glass rod to evenly disperse the metal onto the support. For instance, to prepare 2.5 g of 5% cobalt on silica, 0.9 g of cobalt(II) nitrate hexahydrate was dissolved in ~5 g of distilled water and dispersed in 2.375 g of silica.

Once evenly dispersed onto the support, the catalyst was transferred to a ceramic crucible and placed uncovered in a muffle furnace at 120 ℃ (ramp rate of 5 ℃/min) for 12 h (in a flow of air at 50 mL/min) and then calcined at 450 ℃ for 5 h (ramp rate of 4 ℃/min) before allowing it to cool to room temperature. The catalysts were stored in a desiccator and used in the reaction without pre-treatment unless otherwise stated.

2.3 Catalyst Characterization

Surface area analysis of the catalyst sample was done on an Autosorb iQ-C-MP EPDM automated gas sorption analyzer (Quantachrome Instruments). Roughly 150 mg of the catalyst sample was used for physisorption analysis in a 6 mm glass cell (with bulb, without rod). The sample was first outgassed at 350 °C for 480 min to remove moisture and other adsorbates. Nitrogen physisorption was performed using standard parameters - 40 adsorption/desorption points ranging from partial pressures of 0.025 to 0.995. Then BET analysis was performed on the isotherm data, using adsorption data points from partial pressures of .05 to .35, resulting in the given surface area. The crystalline structure of the catalyst was analyzed using X-ray diffraction (XRD, Rigaku MiniFlex 6G) from 5-90° at a step rate of 0.01 and scan rate of 5°/min.

2.4 Catalyst Testing

The hydrogenolysis reactions were carried out in a 100 mL stainless-steel Parr® reactor equipped with a stainless-steel stirrer, where the catalyst was in contact with polyolefins in the melt-phase under reaction conditions (substrate/catalyst ratio of 10, typically 1.0 g of the substrate and 0.1 g of the catalyst) between 200-300 °C (ramp rate of 5-10 °C/min), 10-40 bar H_2, and 2-36 h catalyst contact time (reaction time). Unless otherwise stated, the reactions were carried out in a borosilicate liner supplied by Parr® to create an inert reaction surface. The borosilicate liner was topped with a custom-made concave PTFE ring that created a seal of the annular region between the liner and the reactor vessel. The actual reactor volume using this setup was 85 mL. The volume was determined by pressurizing the reactor with N_2 to 20 bar and then allowing the gas to expand into an evacuated stainless-steel pipe of a known volume (~58 mL), noting the final pressure, and utilizing ideal gas law to estimate the volume inside the reactor. The reactor was heated using a rigid heating quartz fabric mantle hosted in an aluminum housing and controlled by the Parr® 4848 temperature controller. The stirring speed was 200 rpm to ensure optimal mass transfer (see **Table A.1**). The selection of the stirring speed was made to achieve optimal catalyst contact and minimize mass transfer limitations. Specifically, very high stirring rates (>400 rpm) caused ineffective catalyst contact, i.e., splashing of the catalyst onto the reactor walls and low conversion, while no stirring resulted in low conversion due to ineffective mass transfer. The substrate and catalyst were loaded into the liner and shaken until evenly mixed. The liner was placed inside the reactor, followed by the PTFE ring, before closing. The reactor was purged three times with N_2 and thrice with H_2 at 40 bar and then charged with H_2 to the initial pressure (typically 30 bar).

The time, t=0, was considered when the reaction temperature was reached. After the specified reaction time, the temperature controller was stopped, and the reaction was quenched by dipping the reactor vessel in an ice bath.

2.5 Reaction Workup

Once quenched to ~10 ℃, the gaseous products in the headspace of the reactor were captured in a homemade gas sampling tube (a ~58 mL stainless-steel pipe mounted with a pressure gauge) for analysis. The end products without gas were mixed with 20 mL of ethyl acetate as the solvent and 0.1 g of benzene as an external standard. The reactor was sealed and heated to 150 ℃ for one hour under stirring to effectively dissolve all liquid products in the liner and those trapped in any cold spots in the headspace of the reactor. After cooling to room temperature, the mixture was filtered, and a small aliquot of the liquid was captured in a gas chromatography vial for analysis. The solid residue captured in the filter paper and that left in the liner was dried in an oven at 80 ℃ and weighed separately. To capture any liquid products that may have been condensed in the reactor vessel (outside the borosilicate liner), a second liquid extraction was done using another 20 mL of ethyl acetate and 0.1 g of benzene. The liquids were again filtered, and an aliquot of the liquid was captured.

2.6 Product Analysis

A gas chromatograph (GC) system equipped with a mass spectrometer (MS) and a flame ionization detector (FID) detector (Agilent 8890) was used for the identification and quantification of all products. The gaseous product was injected into the GC (GS-GasPro 60 m x 320 μm x 0 μm column) through a gas sampling valve from the gas sampling tube at least four times for each

sample, and the averaged signals were reported. Gas calibrations were performed using known concentrations of methane in H_2. Other gaseous products (ethane, propane, butane, pentane, and hexane) were quantified with reference to methane using relative response factors (**Table A.2**). The total amount of gas was calculated using the ideal gas law. The liquid products were injected into the GC (HP-5 30 m x 320 μm x 0.25 μm column) using an autosampler (volume of 2 μL). Product quantification was achieved using an octadecane calibration using benzene as an internal standard. The quantities of liquid products (C_5 through C_{30}) were calculated using the relative response factor method with reference to octadecane (**Table A.3**). Liquid compounds heavier than C_{30} were lumped together as C_{30+} hydrocarbons, and branched alkanes were identified as those peaks that appeared in front of each linear alkane peak on the FID detector. The solid residue was determined by subtracting the initial catalyst mass from the total solids remaining in the liner and the filter papers. All conversions, yields, and carbon balances were reported on a carbon mole (C-mol) basis. The small masses not captured in the liquid phase or the solid residue were assumed to be heavy hydrocarbons (C_{30+}) referred to as waxes. The carbon balance was calculated as:

$$C_{captured} = \frac{C_g + C_l + C_s}{C_{sub}} \times 100\ \%$$

Where C_{sub}, C_g, C_l, C_s, and $C_{captured}$ are the amounts (C-mol) of the substrate, gas, liquid, and solid, and total captured products, respectively. The amount of waxes and individual carbon number yields were calculated as:

$$C_w = (1 - C_{captured}) \times 100\ \%$$

$$Y_z = \frac{C_z}{C_{sub}} \times 100\ \%$$

The yield for pentane (C_5) was summed over the gaseous and liquid phases.

2.7 Catalyst Recycling

Post-reaction catalysts were obtained from the solid residue of the previous reaction and charged into the subsequent reaction. In another experiment, the post-reaction catalyst was regenerated by transferring the solid residue from a previous reaction into a ceramic crucible and calcining them at 450 ℃ for 5 h using a ramp rate of ~4 ℃/min in an air flow of 50 mL/min. The regenerated catalyst was then charged into the reactor with identical reaction conditions while maintaining the same catalyst-to-substrate ratio of 1:10.

3. RESULTS AND DISCUSSION[3]

3.1. Catalyst Screening

Catalyst screening tests were done to baseline the performance of ruthenium and the candidate active metals. The active metals screened were Ru, Pt, Pd, Fe, and Co. All catalysts were synthesized using the incipient wetness impregnation method described in the experimental section. Neutral support, silica, was used to evaluate the catalytic performance of the metals and their oxides without any metal-support interaction.[77] Supported ruthenium (Ru) and platinum (Pt)-based catalysts such as Ru/SiO_2, Ru/C, Ru/CeO_2, Ru/TiO_2, Pt/W-β have been shown to be active for the hydrogenolysis of polyolefins, and liquid alkanes (e.g., *n*-octadecane).[77-81, 10, 49-51] While Ru and Pt-based catalysts have received immense interest for the hydrogenolysis of polyolefins, base-metal catalysts such as Cobalt (Co) have shown to be active for the hydrogenolysis of C-C bonds in small linear alkanes have received limited interest for the hydrogenolysis of polyolefins.[82-84] Therefore, an initial series of silica (SiO_2)-supported transition metal (Ru, Pt, Pd, Fe, and Co) catalysts were evaluated for the hydrogenolysis of *n*-octadecane (*n*-C_{18}), a model linear liquid alkane at 200 °C, 30 bar H_2, 2 h, and a catalyst-to-substrate ratio of 1:20 (2.0 g *n*-C_{18}, 0.1 g catalyst). The synthesized Co/SiO_2 catalyst had a BET surface area of ~379 m^2/g. The initial loading of the catalysts was based on 5 wt % loading of the pre-reaction phase (i.e., 5 wt % of RuO_2, Fe_2O_3, Co_3O_4 for Ru, Fe, and Co, respectively, and 5 wt % of Pt and Pd for Pt and Pd, respectively). In line with previous reports by Vlachos and coworkers, Roman-Leshkov and coworkers, and Szanyi and coworkers,[39, 59, 78] Ru/SiO_2 completely converted *n*-C_{18} into methane (CH_4). ~96% yield of methane on a C-mol basis was produced by Ru/SiO_2, while Pd/SiO_2 and

[3] This section is from a manuscript in-preparation. Borkar, S. S., Helmer, R., & Shetty, M. (2023). "Reactivity Investigation and Mechanistic Insights for the Hydrogenolysis of Polyethylene over Silica-supported Earth-abundant Cobalt Catalysts" ACS Sustainable Chemistry & Engineering.

Fe/SiO_2 showed negligible hydrogenolysis reactivity, *i.e.*, C_1-C_{17} yields of <1 C-mol%. Notably, Pt/SiO_2, a widely used catalyst for the hydrocracking of polyolefins, showed only ~3% yields towards hydrogenolysis products from *n*-C_{18}, showing its low propensity for hydrogenolysis. Interestingly, the base-metal Co/SiO_2 converted ~29.5% yield towards C_1-C_{17} alkanes from *n*-C_{18} (~16.2% C_5-C_{17} liquid products and 13.3% C_1-C_5 gas products). **Figure 8** shows the *n*-C_{18} hydrogenolysis product distribution over Co/SiO_2, and

Table 2 shows the yields from the catalyst screening runs.

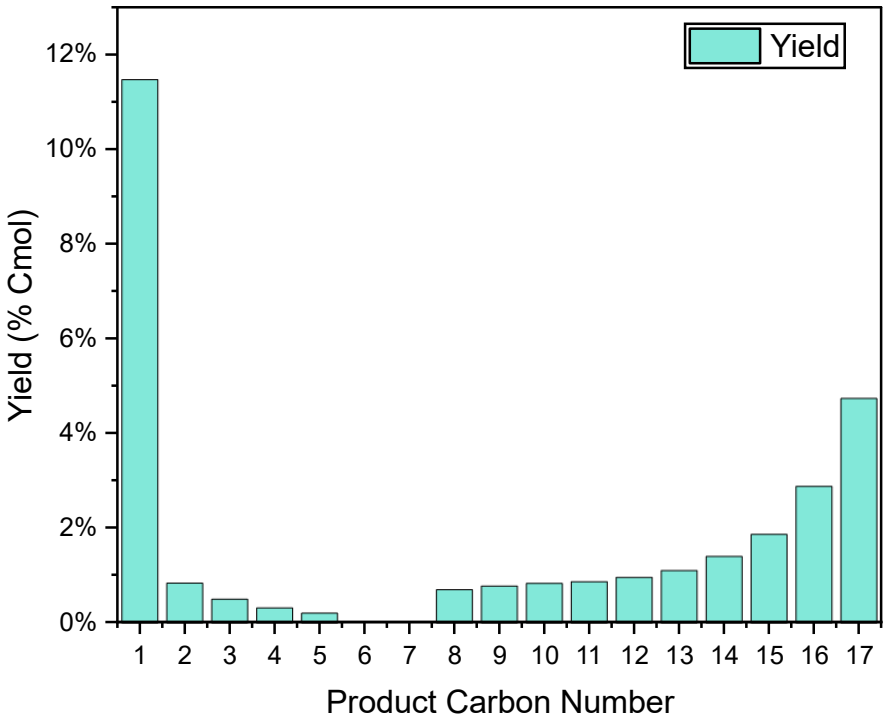

Figure 8. Product yields in % C-mol of *n*-C_{18} hydrogenolysis over Co/SiO_2. Reaction conditions: 200 °C, 30 bar initial H_2, 2 h, 100 RPM, 2.0 g *n*-C_{18}, and 0.1 g Co/SiO_2.

While the noble-metal Ru/SiO_2 showed the highest reactivity, the base-metal Co/SiO_2 showed appreciable reactivity to *n*-C_{18} hydrogenolysis. Considering the potential of replacing noble metal hydrogenolysis catalysts with earth-abundant Co catalysts and preliminary results with

n-C_{18} hydrogenolysis, Co/SiO_2 was selected for further evaluation for the hydrogenolysis of polyolefins.

Table 2. *n*-C_{18} hydrogenolysis for catalyst screening. Reaction conditions: 200 °C, 30 bar initial H_2, 2 h, 100 RPM, 2.0 g *n*-C_{18}, and 0.1 g M/SiO_2.

Catalyst Active Metal	*n*-C_{18} residue (% C-mol)	C_5-C_{17} (liquid) yield (% C-mol)	C_1-C_5 (gas) yield (% C-mol)
Pd	86.75%	0.00%	0.06%
Pt	86.18%	2.12%	0.66%
Fe	92.32%	0.00%	0.00%
Co	55.93%	16.20%	13.33%
Ru	0.00%	0.00%	96.98%

3.2. Effect of Reaction Conditions on PE Hydrogenolysis

The effect of temperature on the hydrogenolysis of a model polyethylene (M_w 4000g/mol, Sigma-Aldrich) on Co/SiO_2 between 200-300 °C was first investigated to identify suitable reaction temperatures at ~30 bar H_2 initial pressure for 4 h (**Figure 9**). At all temperatures, the products consisted of C_1-C_5 light alkanes denoted as gases, C_5-C_{30+} alkanes captured in the liquid denoted as liquids, solid residues denoted as solids or C_{30+} hydrocarbons which precipitate out of the ethyl acetate solution and are not detected in the GC denoted as waxes. The waxes were ascribed to hydrocarbons with large carbon numbers (C_{30+}) that dissolved in the solvent and were undetected in the GC. As the products of interest were primarily in the gas and liquid phases, the solid residue was considered an indication of substrate conversion. As shown in **Figure 9 (a)**, the catalyst showed low conversion at 200 and 225 °C, as seen from the solid yield greater than ~87%. At 200

°C, only ~10% yield towards liquids was observed. At 225°C, ~10% yield towards waxes and ~1% yield towards liquids and gases were seen. As the temperature was raised from 225 °C to 300 °C, the conversion of polyethylene increased, as seen from the decreased solid yields from ~87% at 225 °C to 0% solids at 300 °C. In general, at all temperatures, methane (CH_4) was the dominant gaseous product (**Figure 9(c)**), while the liquid phase products were distributed across the entire range from C_5-C_{30}. **Figure 9(b)** shows the liquid phase product distribution at 250 °C, 275 °C, and 300 °C. The product distributions at 250 °C and 275 °C were similar, with the latter temperature producing ~2.5 times more liquids (~9% and ~25% yield to liquid at 250°C and 275°C, respectively). At 300 °C, along with the complete conversion of polyethylene, ~41% yield to liquids and ~46% yield to gases were observed (**Figure 9(a)**). Interestingly, lower alkanes were favored along with the high liquid yields at 300 °C **(Figure 9(b))**. Notably, ~90% of liquids were in the gasoline and diesel (C_5-C_{20}) range **(Figure 9(d))** as compared to ~52% and ~60% at 250 °C and 275 °C, respectively. This was further reflected in the average carbon number of 21.1, 24.3, and 13.5 at 250 °C, 275 °C, and 300 °C, respectively **(Figure 9(d)).**

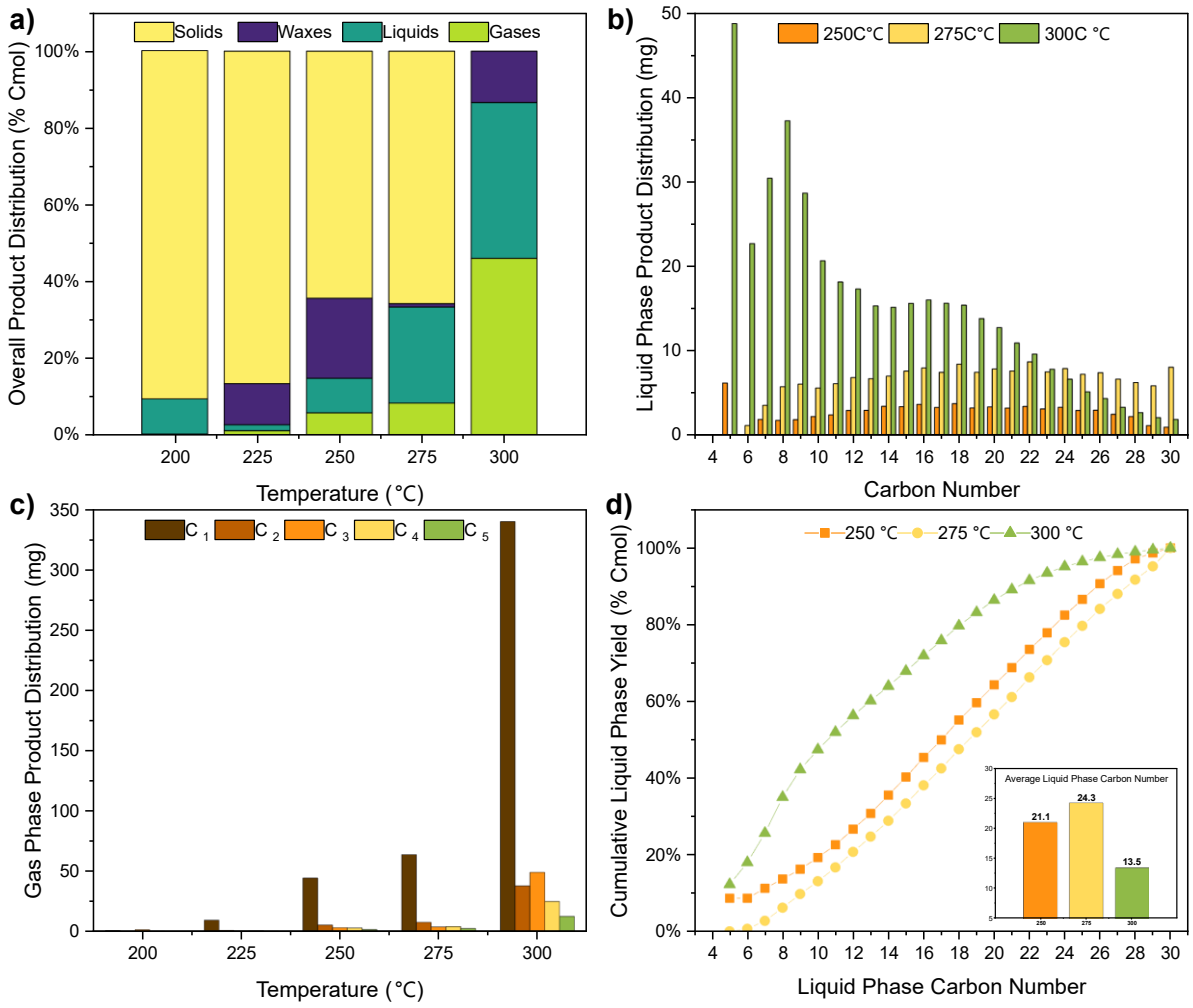

Figure 9. Effect of temperature on PE hydrogenolysis over Co/SiO_2. a) Overall product distribution (% C-mol), b) liquid phase product distribution (m*g*), c) gas phase product distribution (mg), and d) cumulative liquid phase product yield and average liquid phase carbon number. Reaction conditions: 200-300 °C, 30 bar initial H_2, 4 h, 200 RPM, 1.0 g PE, and 0.1 g Co/SiO_2.

Next, the PE hydrogenolysis reactivity of Co/SiO_2 at 275 °C between 20-40 bar initial H_2 pressure was investigated. 275 °C was selected to compare the effect of pressure at less than 100% conversion. It was calculated that a ~20.5 bar H_2 pressure at room temperature was required for the complete conversion of the 1.0 g of PE substrate to CH_4. As shown in **Figure 10**, at 20 bar and 30 bar H_2 and 275 °C, the overall product yields and liquid phase product distributions were similar. Specifically, 5-10% liquid yields and 25-30% gas yields were observed at these pressures. The average total and liquid carbon numbers were ~18 and ~24, respectively (**Figure 10(d)**). As the H_2 pressure was increased to 40 bar, PE showed complete conversion (0% solid yields), and the gas-phase and liquid-phase yields were ~48% and ~27%, respectively. Notably, the liquid phase distribution showed a higher yield of lower carbon numbers and a bimodal distribution (**Figure 10(b)**). The branched product fraction among the liquids was ~ 5% at all H_2 pressures (**Figure 10(d)**). Interestingly at 40 bar H_2 pressure, ~80% of total liquid carbons were in the gasoline and diesel range (C_5-C_{20}), which was reflected in the lower average liquid phase carbon number of ~16 as compared to an average liquid carbon number of ~24 at 20 and 30 bar H_2 pressures (**Figure 10(d)**).

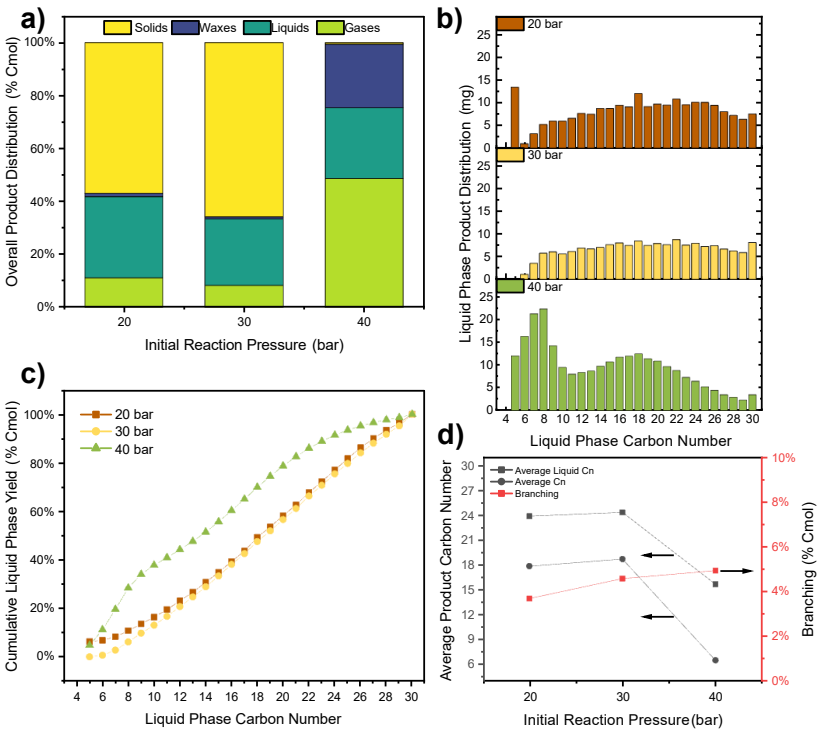

Figure 10. Effect of pressure on PE hydrogenolysis over Co/SiO_2. a) Overall product distribution (% C-mol), b) liquid phase product distribution (mg), c) cumulative liquid phase yield (% C-mol), and d) branching and average product carbon numbers. Reaction conditions: 275 °C, 20-40 bar initial H_2, 4 h, 200 RPM, 1.0 g PE, and 0.1 g Co/SiO_2.

Next, the reaction time was varied from 2 h to 36 h to investigate the effect of reaction time on liquid and gas yields and product distributions at 275 °C and 30 bar H_2 pressure **(Figure 11)**. As shown in **Figure 11(a)**, with an increase in reaction time from 2 to 36 h, the conversion of PE steadily increased. This was reflected in the reduction of solid yields from 70% at 2 h to 0% at 36 h. The liquid yield increased from ~24% to ~58% as the reaction time increased from 2 h to 8 h, then decreased to ~35% and ~2% as the reaction time increased to 16 h and 36 h, respectively. The liquid products show a broad carbon number distribution between reaction times of 2 – 8 h (**Figure 11(b)**). At 16 h, the liquid product distribution was bimodal, with two peaks in the hydrocarbon ranges of gasoline (C_6-C_{12}) and motor oil (C_{20}-C_{30}).[85] As shown in **Figure 11(d)**, between 2 - 16

h, 40-50% of liquid products were in the gasoline and diesel-fuel range, with the rest in the motor-oil (C_{20}-C_{30}) range. **Table 3** shows the recovered yields of the various petroleum fractions over the time series. This was also reflected in the average liquid phase carbon number, which was consistently between ~22-24 (**Figure 11(e)**), while the percentage of branches hydrocarbons in the liquid phase increased monotonically from ~4% to ~15% from 2 to 16 h. In contrast, the gas yield steadily increased with the reaction time, from 7% at 2 h to ~89% at 36 h (**Figure 11(a)**). The average carbon number of the product drops from an initial value of ~18 at 2 and 4 h to ~1.5 at 36 h. This is due to the increasing gas product yields, with the gas product comprising almost exclusively methane at 36 h. Intriguingly, in the gas phase, the yield of C_2-C_5 peaked at 16 h and then dropped to 0 at 36 h, while the methane yield increased monotonically (**Figure 11(c)**). The data showed that reaction temperature, pressure, and time can control the product distribution and conversion of the model polyethylene on Co/SiO_2 catalysts.

Table 3. Recovered yields in % C-mol of various product fractions by PE hydrogenolysis. Reaction conditions: 275 °C, 30 bar initial H_2, 2 – 36 h, 200 RPM, 1.0 g PE, and 0.1 g Co/SiO_2.

Hydrogenolysis Products		Yield (% C-mol)				
Fraction	C_n	2 h	4 h	8 h	16 h	36 h
Methane	1	5.10%	6.35%	16.66%	29.56%	89.46%
Light gases	2-5	1.84%	1.78%	2.86%	5.47%	0.00%
Gasoline	5-12	4.37%	3.71%	9.92%	6.07%	0.00%
Jet fuels	13-15	2.30%	2.11%	6.49%	1.31%	0.00%
Diesel	16-21	5.12%	4.63%	13.42%	7.47%	0.07%
Motor Oil	22-30	6.63%	6.49%	18.18%	16.16%	1.70%
Lubricants	30+	6.05%	8.37%	10.55%	5.34%	0.17%

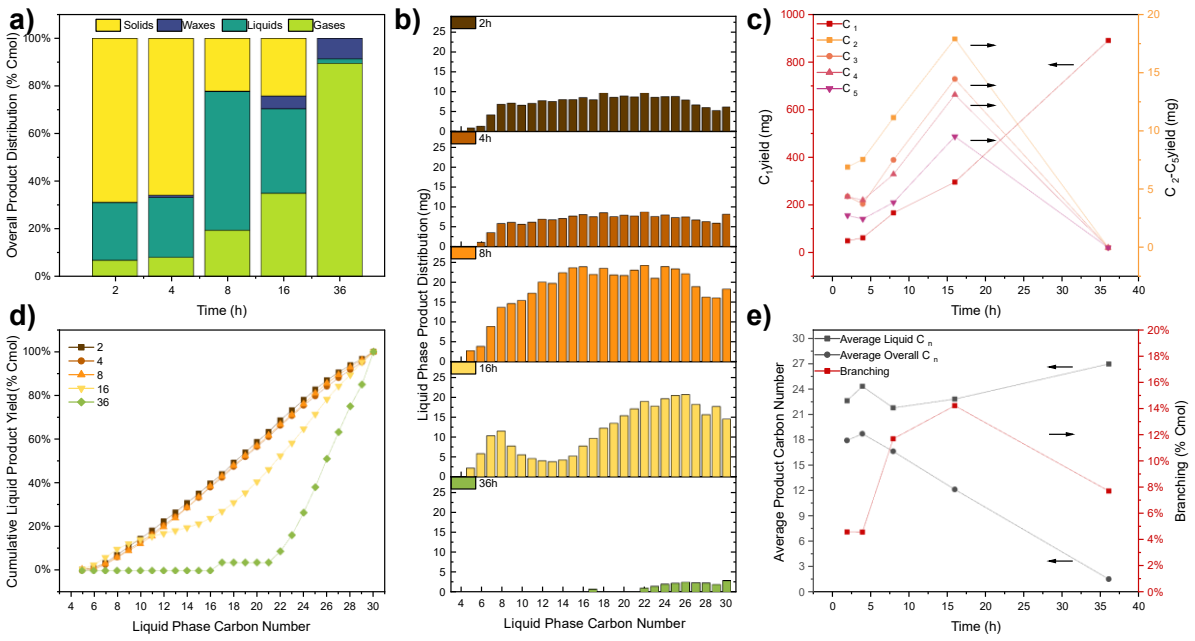

Figure 11. Effect of reaction time on PE hydrogenolysis over Co/SiO_2. a) Overall product distribution (% C-mol), b) liquid phase product distribution (mg), c) gas phase product distribution (mg), d) cumulative liquid phase yield (% C-mol), and e) average product carbon numbers and liquid phase product branching (% C-mol). Reaction conditions: 275 °C, 30 bar initial H_2, 2 – 36 h, 200 RPM, 1.0 g PE, and 0.1 g Co/SiO_2.

The hydrogenolysis reaction can take several possible routes based on the C-C bond cleavage location along the PE backbone (**Figure 12**). First, in the terminal cleavage route, the final C-C bond at the ends of the polyolefin chains undergoes dehydrogenative adsorption on the metal site, followed by C-C cleavage, which forms methane and the polyolefin with one less carbon atom, which all then desorb from the surface. The polymer chain end is progressively cleaved with successive secondary and tertiary events, steadily increasing the CH_4 yield. On the other hand, the sequential non-terminal cleavage route involves dehydrogenative adsorption of random, internal C-C bonds away from the chain ends, forming fragmented polyolefin chains as the primary products, which then desorb. After that, secondary and tertiary events independently

occur on the daughter polyolefin chains, forming a variety of hydrocarbons, which eventually form CH_4 as the products are cleaved further.

The terminal and non-terminal cleavage routes assume that hydrogenolysis occurs as discrete events, with only one C-C bond cleaving at a given time. However, it is also possible for several C-C bonds to cleave simultaneously, especially if there were a significant number of active metal sites in proximity. As such, a tandem non-terminal cleavage route is proposed, as shown in **Figure 12**, with multiple simultaneous C-C bond cleavages. Due to the long, rope-like structure of the polyolefin chain, it is likely that if one point meets the catalyst surface, several nearby points on the chain also contact the surface. It is postulated that the polymer weakly adsorbs (physisorption) to the silica surface at multiple nearby locations along a chain segment, with metal sites intermittently located along the segment. The chain dehydrogenates, cleaves, and ultimately desorbs at these metal sites. The scission at these sites need not happen synchronously, but rather the proximity of these sites will result in oligomer-length segments that produce lower hydrocarbons in the C_2-C_{30} range once released. These hydrocarbons could undergo further hydrogenolysis in the secondary and tertiary events, eventually forming methane.

In the tandem non-terminal cleavage route, before multiple secondary and tertiary events occur, the yield of liquid range or oligomeric hydrocarbons would be greater than that of light gases, particularly methane. The time series above suggests that the degree of terminal C-C bond hydrogenolysis is lower than non-terminal cleavage on Co/SiO_2 catalysts, as seen in the higher liquid selectivity at lower conversions as oligomers form first and subsequently degrade to gases.

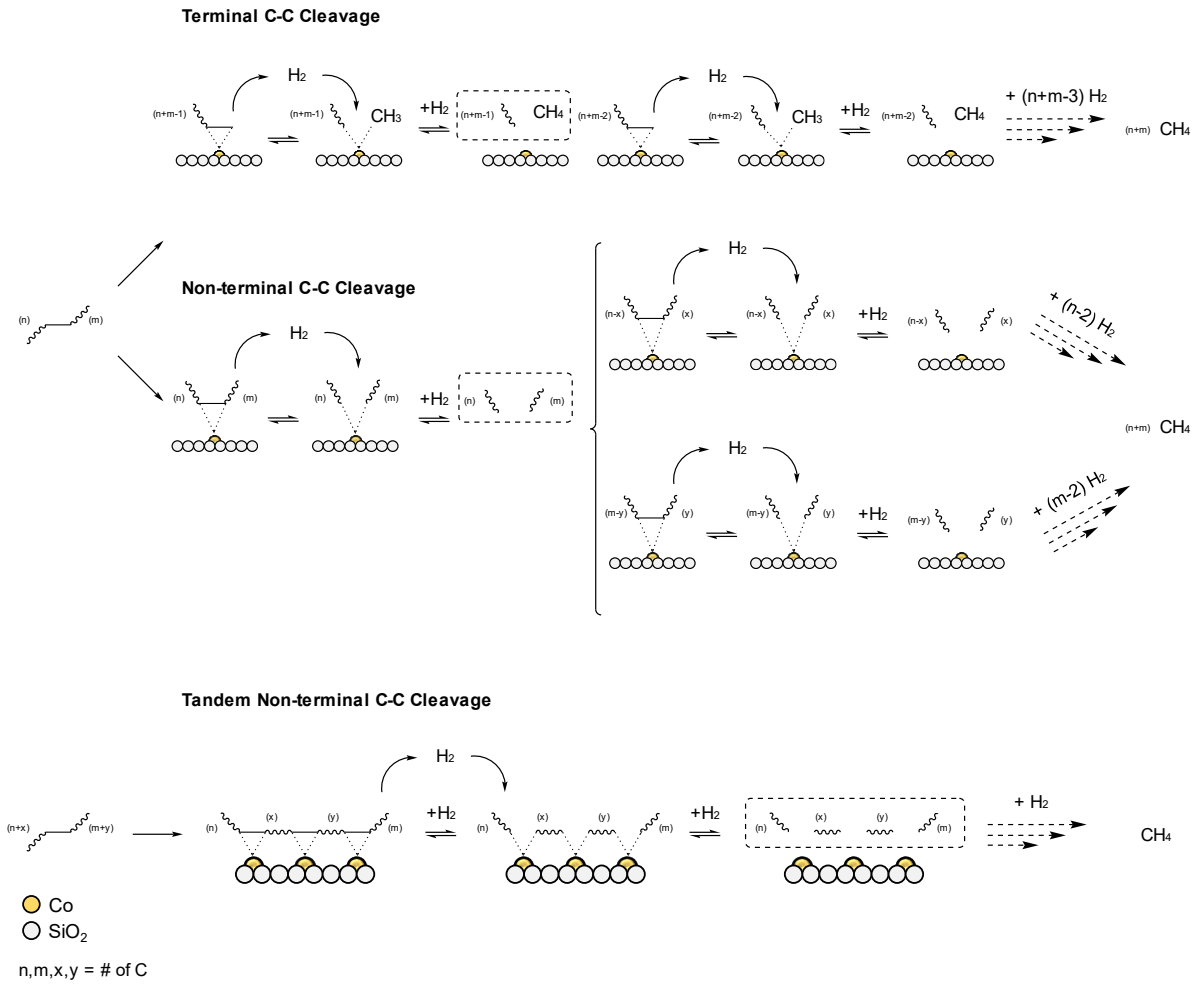

Figure 12. Mechanistic routes of PE hydrogenolysis. PE hydrogenolysis can take three routes: i) terminal C-C cleavage, wherein primary events form methane and a PE chain with one carbon less, while secondary and tertiary events form sequentially lower alkanes and eventually all methane, ii) non-terminal C-C cleavage, wherein primary events form two oligomeric hydrocarbons and secondary and tertiary events on the daughter hydrocarbons form lower alkanes, eventually forming methane, and iii) tandem non-terminal C-C cleavage, wherein the PE chain adsorbs onto several active metal sites and simultaneously cleaves into several daughter oligomeric hydrocarbons, which then undergo further hydrogenolysis, eventually forming methane.

Furthermore, the broad liquid distribution and the average total carbon number remain stable for the first 4 h (**Figure 11(b, e)**) further support the hypothesis, namely that these oligomers are being produced at a steady rate while reactant species are not limited. The steady increase in

C_2-C_5 gases indicated secondary non-terminal C-C cleavage events, and their eventual conversion into CH_4 confirmed tertiary events. The near-zero CH_4 yields at low reaction times further suggest that terminal C-C cleavage is a minor route (**Figure 11(c)**).

In the tandem non-terminal cleavage route, before multiple secondary and tertiary events occur, the yield of liquid range or oligomeric hydrocarbons would be greater than that of light gases, particularly methane. The time series above suggests that the degree of terminal C-C bond hydrogenolysis is lower than non-terminal cleavage on Co/SiO_2 catalysts, as seen in the higher liquid selectivity at lower conversions as oligomers form first and subsequently degrade to gases. Furthermore, the broad liquid distribution and the average total carbon number remain stable for the first 4 h (**Figure 11(b, e)**) further support the hypothesis, namely that these oligomers are being produced at a steady rate while reactant species are not limited. The steady increase in C_2-C_5 gases indicated secondary non-terminal C-C cleavage events, and their eventual conversion into CH_4 confirmed tertiary events. The near-zero CH_4 yields at low reaction times further suggest that terminal C-C cleavage is a minor route (**Figure 11(c)**).

To investigate this further, a catalyst loading study was conducted, varying the concentration of the active metal in the silica support. In addition to the 5 wt % catalyst, 1 and 10 wt % catalysts (herein referred to as 1-Co/SiO_2, 5-Co/SiO_2, and 10-Co/SiO_2) were synthesized and employed in the reaction at 275 C and 30 bar initial H_2. The substrate-to-active metal ratio was kept constant, meaning only the active site density and the total catalyst mass varied. **Figure 13** shows the product distributions of PE hydrogenolysis using comparing these loadings over the first 8 h of the reaction.

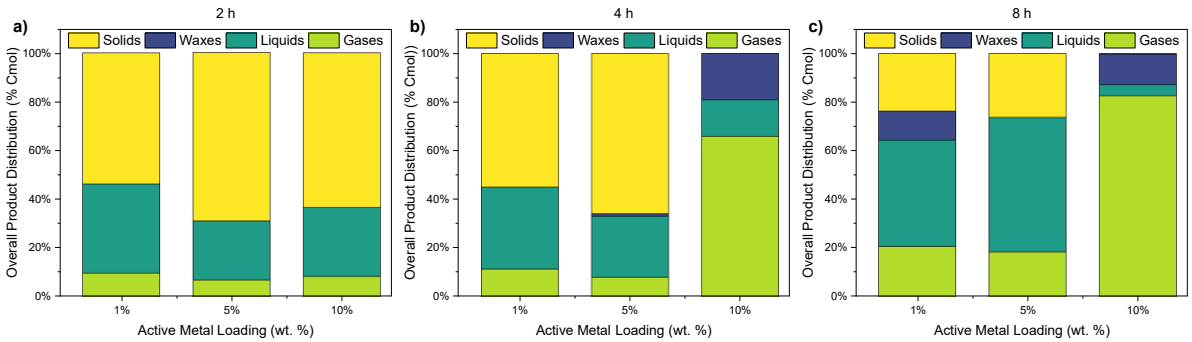

Figure 13. Effect of active metal loading on PE hydrogenolysis over Co/SiO_2. Overall product distributions (% C-mol) at a reaction time of a) 2 h, b) 4 h, and c) 8 h. Reaction conditions: 275 °C, 30 bar initial H_2, 4 h, 200 RPM, 1.0 g PE, and 0.5 g 1 wt % Co/SiO_2 , 0.1 g 5 wt % Co/SiO_2, or 0.05 g 10 wt % Co/SiO_2.

At 2 h, where the solid conversion was low, the three loadings gave similar product distributions. 1-Co/SiO_2 showed slightly higher conversion, possibly due to relatively better catalyst-to-substrate contact due to the greater total catalyst mass. At 4 h, while 1- and 5-Co/SiO_2 had only slightly greater conversion (in line with the earlier presented time series), 10-Co/SiO_2 converted all the substrate into majorly gaseous products. At a longer time of 8 h, liquids were the dominant product in 1- and 5-Co/SiO_2, while 10-Co/SiO2 predominantly produced gases. This loading study further substantiates the hypothesis of discrete non-terminal and tandem non-terminal C-C bond cleavages over Co/SiO_2. Specifically, a higher active site density favors the tandem routes wherein several C-C cleavages co-occur, giving a variety of oligomeric products at first, which then rapidly degrade into gases in subsequent events. On the other hand, a lower active site density limits the number of simultaneous C-C bond cleavages, steadily increasing the production of oligomers before attaining a peak and degrading into gases. As such, a specific active metal can drive product selectivity and develop a mechanistic understanding of the reaction.

It has recently been hypothesized that bulk Co_3O_4 favored terminal C-C bond cleavage in PE hydrogenolysis[75], and observations from this study suggest that immobilizing Co_3O_4 on a neutral support shifts its preference from terminal to non-terminal cleavage. As such, it is postulated that the first step of the hydrogenolysis reaction mechanism, the dehydrogenative adsorption of the C-C bond on the metal, is regiosensitive and that the probability of its occurrence at different locations along the PE backbone is not uniform.

3.3. Catalyst Recyclability

Recyclability of the catalyst with and without calcination between subsequent runs was tested. These were tested first by reusing the catalyst without any treatment between runs and next by calcining the catalyst between reactions at 450 °C for 12 h. These reactions were carried out at 300 °C, 30 bar H_2 for 4 h to maximize the solid conversion and enable the easy extraction of the catalyst post-reaction. It was assumed that the post-reaction solids were predominantly catalysts. The solids were directly added to the subsequent run to test the catalyst's direct reuse, while the PE substrate mass was kept the same (1.0 g). It must be noted that there was about a 10% catalyst mass loss between each run. **Figure 14(a)** shows that largely gaseous hydrocarbons (~80% yield) were produced using the virgin catalyst. The catalyst was reused 3 more times. During the first reuse, the liquid products were favored with ~53% yields with ~18% and ~29% gas and wax yields, respectively. These product yields remained essentially unchanged in each subsequent run.

Alternatively, to evaluate the catalyst's recyclability, the post-reaction catalyst was calcined before being used for the subsequent run. In this study, the catalyst-to-substrate ratio was maintained at 1:10. The regenerated catalyst produced a similar product (~46% gas, ~20% liquid, ~31% wax, and ~3% solid yields) distribution as compared to the virgin catalyst (~50% gas, ~22%

liquid, and ~28% wax yields). These two comparative studies showed that Co/SiO_2's hydrogenolysis activity decreases when reused without treatment, which can be attributed to either catalyst deactivation through carbon deposition or an *in-situ* change in the metal's phase (due to the high temperature reducing H_2 environment) leading to an inherent change in catalyst activity. This change is, however, reversible, and the catalyst's activity can be restored by post-reaction calcination. Further, our observations suggest that the change in activity is not progressive either, meaning that after the first run, the catalyst can be reused several times to give a similar product distribution. These attributes can be leveraged in optimizing process design.

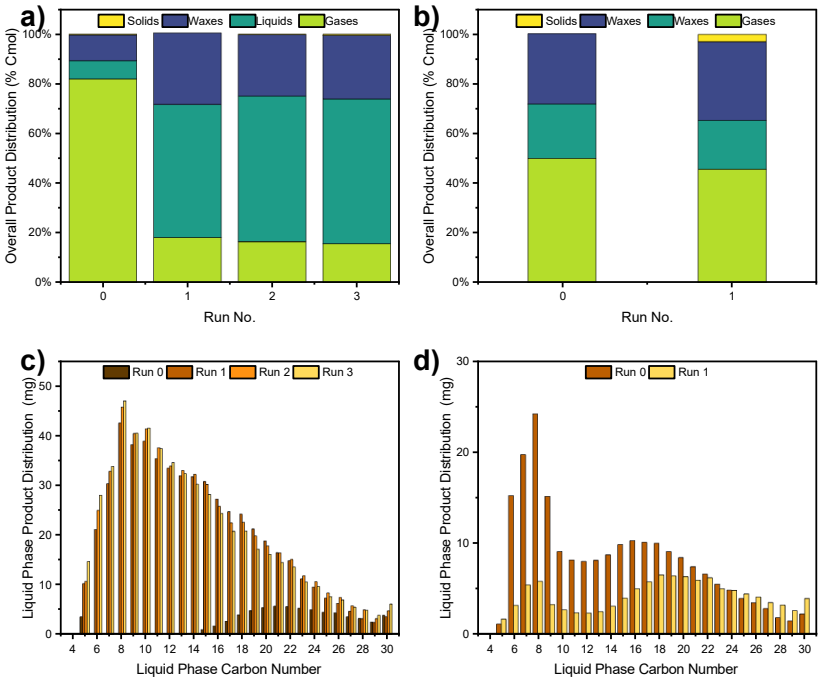

Figure 14. Recyclability of Co/SiO_2 catalyst in PE hydrogenolysis. Overall product distribution (% C-mol) of a) catalyst reuse runs and b) catalyst regeneration runs, and liquid-phase product distribution (mg) of c) catalyst reuse runs and d) catalyst regeneration runs. Reaction conditions: 300 °C, 30 bar initial H_2, 4 h, 200 RPM, 1.0 g PE in all reuse runs and regeneration run 0, and ~0.55 g substrate in regeneration run 1, 0.1 g Co/SiO_2 in both runs 0 and all recovered catalyst in subsequent runs.

To determine the active phase of the catalyst under reaction conditions and investigate the reason for the change in product distribution in reuse data, PXRD was conducted for the catalyst samples pre- and post-reaction from the 16 h run with the 5 wt % Co/SiO_2 (5-Co/SiO_2), the 8 h run with the 10 wt % Co/SiO_2 (10-Co/SiO_2) , and the recovered 5-Co/SiO_2 after the third resuse run (**Figure 15**).

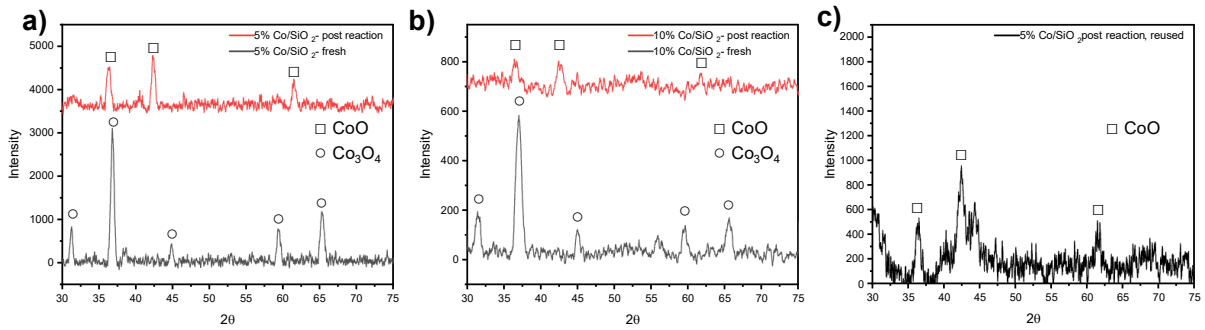

Figure 15. Pre- and post-reaction powder X-ray diffraction patterns of Co/SiO_2. Reaction conditions: a) 275 °C, 30 bar initial H_2, 16 h, 200 RPM, 1.0 g PE, and 0.1 g 5-Co/SiO_2 and b) 275 °C, 30 bar initial H_2, 8 h, 200 RPM, 1.0 g PE, and 0.05 g 10-Co/SiO_2. c) 300 °C, 30 bar initial H_2, 4 h, 200 RPM, 1.0 g PE, and 0.1 g initial 5-Co/SiO_2.

First, the pre-reaction catalyst showed diffraction patterns corresponding to Co_3O_4 for both active metal loadings. For both post-reaction samples, peaks at 2Θ values corresponding to lattice planes of CoO were seen, along with the Co_3O_4 peaks having disappeared, confirming that the catalyst underwent *in-situ* reduction during the reaction. Further, the peak locations in the post-reaction catalyst sample after the third reuse run (**Figure *15***(c)) are identical to the other post-reaction catalyst samples, suggesting that the catalyst did not undergo any further phase change after the first reaction. These findings reveal that CoO is likely the active phase of the catalyst under reaction conditions. As the post-reaction PXRD patterns are similar for the post-reaction

catalysts, the change in the active phase is not the cause of the change in product yields after the first reaction in the reuse study (**Figure 14**(a)). Therefore, it is postulated that the regeneration through calcination activates the catalyst, likely by removing coke from the catalyst surface.

3.4. Performance of Co/SiO_2 in End-of-Use Plastic Hydrogenolysis

To test the applicability of the catalyst to hydrogenolysis of post-consumer waste polyolefins, end-of-use plastics HDPE (VWR solvent jug), LDPE (packaging bag and VWR solvent bottle), and PP (fruit cups) were introduced. HDPE and LDPE differ in the hydrocarbon backbone's linearity and crystallinity.[86] These substrates were used without purification or pre-treatment. As such, the post-consumer polyolefins had varying impurities, fillers, molecular masses, branching, and crystal structure. The post-consumer polyolefins were contacted with the catalyst at 275 °C, and 30 bar H_2 for 8 h. **Figure 16(a and b)** shows that three different PE substrates yielded similar overall and liquid phase product yields and distributions. Specifically, the solid, gas and liquid yields ranged between 10-30%, 45-60%, and 20-35% for the three PEs. The average liquid phase carbon numbers for all PE substrates fell in a narrow range of C_{20}-C_{22} (**Figure 16(d)**).

The catalyst, however, was not as effective in deconstructing PP as PE, possibly due to the inherently different backbone of the two polyolefins. Interestingly, it was more selective towards liquid-range hydrocarbons than gases. Specifically, the liquid and gas yields were ~33% and ~6%, respectively, under identical reaction conditions. The branched structure of the liquid products would make the hydrogenolysis products good candidates for gasoline blends. Furthermore, gasoline (C_6-C_{12}) and diesel range (C_{13}-C_{20}) hydrocarbons comprise ~40% of total liquid hydrocarbons. The consistent and high activity of the catalyst towards PE hydrogenolysis (vs. PP) could have consequences in the sorting of plastics before hydrogenolysis.[87]

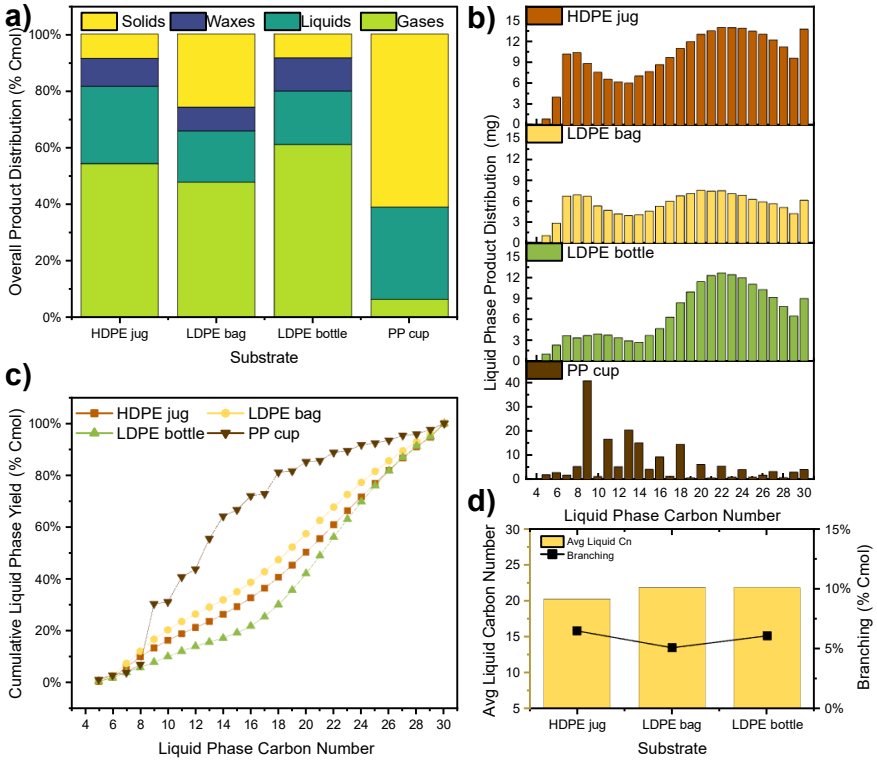

Figure 16. End-of-use plastic hydrogenolysis over Co/SiO_2. a) Overall product yields, b) liquid-phase product mass in mg, and c) cumulative liquid-phase product yield in % C-mol. Reaction conditions: 275 °C, 30 bar initial H_2, 8 h, 200 RPM, 1.0 g substrate, and 0.1 g Co/SiO_2.

4. CONCLUSION AND OUTLOOK

This work explored using 5 wt % silica-supported cobalt (Co/SiO_2) as a promising earth-abundant hydrogenolysis catalyst for converting polyethylenes at mild reaction conditions of 200-300 °C and 20-40 bar H_2. Co was shown to be a promising alternative to the rare-earth Ru for PE hydrogenolysis and how reaction conditions (temperature, initial pressure, and reaction time) can be adjusted to direct its selectivity toward desired hydrocarbon products. At temperatures greater than 275 °C at 30 bar H_2 for 4 h, Co/SiO_2 showed high liquid selectivity over gases (~25% liquid yield and ~8% gas yield). These liquid yields were further optimized at 275 °C and 30 bar H_2 at 8 h to selectively produce ~58% liquid and 19.5% gas yield, respectively, with an average liquid C_n=21.8 from a model PE substrate of M_w=4,000 g/mol. The product yields with varying reaction times and catalyst (i.e., Co) loadings showed that the catalyst showed regioselectivity toward non-terminal C-C bond cleavage compared to terminal C-C bond cleavage.

The catalyst effectively converted real-world PE wastes (HDPE jug, LDPE bag, and LDPE bottle) into liquid and gaseous hydrocarbons (65-81% conversion, 48-61% gaseous, and 18-27% liquid yields at 275 °C, 30 bar H_2, and 8 h). The catalyst showed excellent recyclability, and PXRD analysis revealed that CoO was likely the active phase at the reaction conditions. It was agnostic to impurities, fillers, and additives in the substrates and had comparable product distributions across the different PE substrates.

Future directions on using supported cobalt catalysts for PE hydrogenolysis is in identifying precise parameters, including the choice of support for catalyst design that further drives its regioselectivity toward non-terminal C-C cleavage elucidates the hydrogenolysis reaction mechanism.

REFERENCES

(1) Rahimi, A.; García, J. M. Chemical recycling of waste plastics for new materials production. *Nat. Rev. Chem.* **2017**, *1* (6), 0046.

(2) Geyer, R.; Jambeck, J. R.; Law, K. L. Production, use, and fate of all plastics ever made. *Sci. Adv.* **2017**, *3* (7), e1700782.

(3) Jambeck, J. R.; Geyer, R.; Wilcox, C.; Siegler, T. R.; Perryman, M.; Andrady, A.; Narayan, R.; Law Kara, L. Plastic waste inputs from land into the ocean. *Science* **2015**, *347* (6223), 768-771.

(4) Mark, L. O.; Cendejas, M. C.; Hermans, I. The Use of Heterogeneous Catalysis in the Chemical Valorization of Plastic Waste. *ChemSusChem* **2020**, *13* (22), 5808-5836.

(5) Celik, G.; Kennedy, R. M.; Hackler, R. A.; Ferrandon, M.; Tennakoon, A.; Patnaik, S.; LaPointe, A. M.; Ammal, S. C.; Heyden, A.; Perras, F. A.; et al. Upcycling Single-Use Polyethylene into High-Quality Liquid Products. *ACS Cent. Sci.* **2019**, *5* (11), 1795-1803.

(6) Nicholson, S. R.; Rorrer, N. A.; Carpenter, A. C.; Beckham, G. T. Manufacturing energy and greenhouse gas emissions associated with plastics consumption. *Joule* **2021**, *5* (3), 673-686.

(7) UNEP. *From Pollution to Solution: A global assessment of marine litter and plastic pollution.*; United Nations Environment Programme, Nairobi, 2021.

(8) Wang, C. Y.; Liu, Y.; Chen, W. Q.; Zhu, B.; Qu, S.; Xu, M. Critical review of global plastics stock and flow data. *J. Ind. Ecol.* **2021**, *25* (5), 1300-1317.

(9) Chamas, A.; Moon, H.; Zheng, J.; Qiu, Y.; Tabassum, T.; Jang, J. H.; Abu-Omar, M.; Scott, S. L.; Suh, S. Degradation Rates of Plastics in the Environment. *ACS Sustainable Chem. Eng.* **2020**, *8* (9), 3494-3511.

(10) Zhang, F.; Zeng, M. H.; Yappert, R. D.; Sun, J. K.; Lee, Y. H.; LaPointe, A. M.; Peters, B.; Abu-Omar, M. M.; Scott, S. L. Polyethylene upcycling to long-chain alkylaromatics by tandem hydrogenolysis/aromatization. *Science* **2020**, *370* (6515), 437-441.

(11) Law, K. L. Plastics in the Marine Environment. In *Annual Review of Marine Science*, Vol. 9; 2017; pp 205-229.

(12) Cózar, A.; Echevarría, F.; González-Gordillo, J. I.; Irigoien, X.; Úbeda, B.; Hernández-León, S.; Palma Álvaro, T.; Navarro, S.; García-de-Lomas, J.; Ruiz, A.; et al. Plastic debris in the open ocean. *Proc. NAS* **2014**, *111* (28), 10239-10244.

(13) Belden, E. R.; Kazantzis, N. K.; Reddy, C. M.; Kite-Powell, H.; Timko, M. T.; Italiani, E.; Herschbach, D. R. Thermodynamic feasibility of shipboard conversion of marine plastics to blue diesel for self-powered ocean cleanup. *P Natl Acad Sci USA* **2021**, *118* (46).

(14) Landrigan, P. J.; Stegeman, J. J.; Fleming, L. E.; Allemand, D.; Anderson, D. M.; Backer, L. C.; Brucker-Davis, F.; Chevalier, N.; Corra, L.; Czerucka, D.; et al. Human Health and Ocean Pollution. *Ann Glob Health* **2020**, *86* (1), 151.

(15) van den Bergh, J. C. J. M.; Botzen, W. J. W. Monetary valuation of the social cost of CO2 emissions: A critical survey. *Ecol. Econ.* **2015**, *114*, 33-46.

(16) Schyns, Z. O. G.; Shaver, M. P. Mechanical Recycling of Packaging Plastics: A Review. *Macromol. Rapid Commun.* **2021**, *42* (3).

(17) Chen, X.; Wang, Y. D.; Zhang, L. Recent Progress in the Chemical Upcycling of Plastic Wastes. *ChemSusChem* **2021**, *14* (19), 4137-4151.

(18) Shen, M.; Huang, W.; Chen, M.; Song, B.; Zeng, G.; Zhang, Y. (Micro)plastic crisis: Un-ignorable contribution to global greenhouse gas emissions and climate change. *J. Clean. Prod.* **2020**, *254*, 120138.

(19) Hamilton, L. A.; Feit, S.; Muffett, C.; Kelso, M.; Rubright, S. M.; Bernhardt, C.; Schaeffer, E.; Moon, D.; Morris, J.; Labbe-Bellas, R. *Plastic & Climate: The Hidden Costs of a Plastic Planet*; Center for International Environmental Law, 2019. https://www.ciel.org/plasticandclimate/.

(20) Chen, H.; Wan, K.; Zhang, Y.; Wang, Y. Waste to Wealth: Chemical Recycling and Chemical Upcycling of Waste Plastics for a Great Future. *ChemSusChem* **2021**, *14* (19), 4123-4136.

(21) Jehanno, C.; Alty, J.; Roosen, M.; De Meester, S.; Dove, A.; Chen, E.; Leibfarth, F.; Sardon, H. Critical advances and future opportunities in upcycling commodity polymers. *Nature* **2022**, *603*, 803-814.

(22) Nicholson, S. R.; Rorrer, J. E.; Singh, A.; Konev, M. O.; Rorrer, N. A.; Carpenter, A. C.; Jacobsen, A. J.; Román-Leshkov, Y.; Beckham, G. T. The Critical Role of Process Analysis in Chemical Recycling and Upcycling of Waste Plastics. *Annual Review of Chemical and Biomolecular Engineering* **2022**, *13* (1), 301-324.

(23) Panda, A. K.; Singh, R. K.; Mishra, D. K. Thermolysis of waste plastics to liquid fuel A suitable method for plastic waste management and manufacture of value added products-A world prospective. *Renew. Sust. Energ. Rev.* **2010**, *14* (1), 233-248.

(24) Roy, P. S.; Garnier, G.; Allais, F.; Saito, K. Strategic Approach Towards Plastic Waste Valorization: Challenges and Promising Chemical Upcycling Possibilities. *ChemSusChem* **2021**, *14* (19), 4007-4027.

(25) Beromi, M. M.; Kennedy, C. R.; Younker, J. M.; Carpenter, A. E.; Mattler, S. J.; Throckmorton, J. A.; Chirik, P. J. Iron-catalysed synthesis and chemical recycling of telechelic 1,3-enchained oligocyclobutanes. *Nat. Chem.* **2021**, *13* (2), 156-162.

(26) Shi, C.; Reilly, L. T.; Phani Kumar, V. S.; Coile, M. W.; Nicholson, S. R.; Broadbelt, L. J.; Beckham, G. T.; Chen, E. Y. X. Design principles for intrinsically circular polymers with tunable properties. *Chem* **2021**, *7* (11), 2896-2912.

(27) IEA. *Production of key thermoplastics, 1980-2050*. 2020. https://www.iea.org/data-and-statistics/charts/production-of-key-thermoplastics-1980-2050 (accessed 03/30/2022).

(28) Kots, P. A.; Vance, B. C.; Vlachos, D. G. Polyolefin plastic waste hydroconversion to fuels, lubricants, and waxes: a comparative study. *React. Chem. Eng.* **2022**.

(29) Infantes-Molina, A.; Merida-Robles, J.; Rodriguez-Castellon, E.; Pawelec, B.; Fierro, J. L. G.; Jimenez-Lopez, A. Catalysts based on Co/zirconium doped mesoporous silica MSU for the hydrogenation and hydrogenolysis/hydrocracking of tetralin. *Appl. Catal., A* **2005**, *286* (2), 239-248.

(30) Weitkamp, J. Catalytic Hydrocracking-Mechanisms and Versatility of the Process. *ChemCatChem* **2012**, *4* (3), 292-306.

(31) Liu, S. B.; Kots, P. A.; Vance, B. C.; Danielson, A.; Vlachos, D. G. Plastic waste to fuels by hydrocracking at mild conditions. *Sci. Adv.* **2021**, *7* (17), 9.

(32) Nakaji, Y.; Tamura, M.; Miyaoka, S.; Kumagai, S.; Tanji, M.; Nakagawa, Y.; Yoshioka, T.; Tomishige, K. Low-temperature catalytic upgrading of waste polyolefinic plastics into liquid fuels and waxes. *Appl. Catal., B* **2021**, *285*, 9.

(33) Jia, C.; Xie, S.; Zhang, W.; Intan, N. N.; Sampath, J.; Pfaendtner, J.; Lin, H. Deconstruction of high-density polyethylene into liquid hydrocarbon fuels and lubricants by hydrogenolysis over Ru catalyst. *Chem Catal.* **2021**, *1* (2), 437-455.

(34) Milbrandt, A.; Coney, K.; Badgett, A.; Beckham, G. T. Quantification and evaluation of plastic waste in the United States. *Resour. Conserv. Recycl.* **2022**, *183*, 106363.

(35) EIA, U. *Monthly Energy Review*; U.S. Energy Information Administration, 2022. https://www.eia.gov/energyexplained/use-of-energy/transportation.php.

(36) Dufaud, V.; Basset, J. M. Catalytic Hydrogenolysis at Low Temperature and Pressure of Polyethylene and Polypropylene to Diesels or Lower Alkanes by a Zirconium Hydride Supported on Silica-Alumina: A Step Toward Polyolefin Degradation by the Microscopic Reverse of Ziegler-Natta Polymerization. *Angew. Chem. Int., Ed. Engl.* **1998**, *37* (6), 806-810.

(37) Hongkailers, S.; Jing, Y.; Wang, Y.; Hinchiranan, N.; Yan, N. Recovery of Arenes from Polyethylene Terephthalate (PET) over a Co/TiO2 Catalyst. *ChemSusChem* **2021**, *14* (19), 4330-4339.

(38) Kratish, Y.; Li, J.; Liu, S.; Gao, Y.; Marks, T. J. Polyethylene Terephthalate Deconstruction Catalyzed by a Carbon-Supported Single-Site Molybdenum-Dioxo Complex. *Angew. Chem. Int., Ed. Engl.* **2020**, *59* (45), 19857-19861.

(39) Rorrer, J. E.; Beckham, G. T.; Roman-Leshkov, Y. Conversion of Polyolefin Waste to Liquid Alkanes with Ru-Based Catalysts under Mild Conditions. *JACS Au* **2021**, *1* (1), 8-12.

(40) Almithn, A.; Hibbitts, D. Comparing Rate and Mechanism of Ethane Hydrogenolysis on Transition-Metal Catalysts. *J. Phys. Chem. C* **2019**, *123* (9), 5421-5432.

(41) Flaherty, D. W.; Hibbitts, D. D.; Iglesia, E. Metal-catalyzed C-C bond cleavage in alkanes: Effects of methyl substitution on transition-state structures and stability. *J. Am. Chem. Soc.* **2014**, *136*, 9664.

(42) Mason, A. H.; Motta, A.; Das, A.; Ma, Q.; Bedzyk, M. J.; Kratish, Y.; Marks, T. Facile Polyolefin Plastics Hydrogenolysis Catalyzed by a Surface Electrophilic d0 Hydride. American Chemical Society (ACS): 2021.

(43) Ballarini, A. D.; de Miguel, S. R.; Castro, A. A.; Scelza, O. A. n-Decane dehydrogenation on Pt, PtSn and PtGe supported on spinels prepared by different methods of synthesis. *Appl. Catal., A* **2013**, *467*, 235-245.

(44) Li, H.; Wang, L.; Dai, Y.; Pu, Z.; Lao, Z.; Chen, Y.; Wang, M.; Zheng, X.; Zhu, J.; Zhang, W.; et al. Synergetic interaction between neighbouring platinum monomers in CO2 hydrogenation. *Nat. Nanotechnol.* **2018**, *13* (5), 411-417.

(45) Lucci, F. R.; Liu, J.; Marcinkowski, M. D.; Yang, M.; Allard, L. F.; Flytzani-Stephanopoulos, M.; Sykes, E. C. H. Selective hydrogenation of 1,3-butadiene on platinum–copper alloys at the single-atom limit. *Nat. Commun.* **2015**, *6* (1), 8550.

(46) Sun, G.; Zhao, Z.-J.; Mu, R.; Zha, S.; Li, L.; Chen, S.; Zang, K.; Luo, J.; Li, Z.; Purdy, S. C.; et al. Breaking the scaling relationship via thermally stable Pt/Cu single atom alloys for catalytic dehydrogenation. *Nat. Commun.* **2018**, *9* (1), 4454.

(47) Sun, P.; Siddiqi, G.; Chi, M.; Bell, A. T. Synthesis and characterization of a new catalyst Pt/Mg(Ga)(Al)O for alkane dehydrogenation. *J. Catal.* **2010**, *274* (2), 192-199.

(48) Ertem, S. P.; Onuoha, C. E.; Wang, H. Q.; Hillmyer, M. A.; Reineke, T. M.; Lodge, T. P.; Bates, F. S. Hydrogenolysis of Linear Low-Density Polyethylene during Heterogeneous Catalytic Hydrogen-Deuterium Exchange. *Macromolecules* **2020**, *53* (14), 6043-6055.

(49) Tennakoon, A.; Wu, X.; Paterson, A. L.; Patnaik, S.; Pei, Y. C.; LaPointe, A. M.; Ammal, S. C.; Hackler, R. A.; Heyden, A.; Slowing, II; et al. Catalytic upcycling of high-density polyethylene via a processive mechanism. *Nat. Catal.* **2020**, *3* (11), 893-901.

(50) Wu, X.; Tennakoon, A.; Yappert, R.; Esveld, M.; Ferrandon, M. S.; Hackler, R. A.; LaPointe, A. M.; Heyden, A.; Delferro, M.; Peters, B.; et al. Size-Controlled Nanoparticles Embedded in a

Mesoporous Architecture Leading to Efficient and Selective Hydrogenolysis of Polyolefins. *J. Am. Chem. Soc.* **2022**, *144* (12), 5323-5334.

(51) Vance, B. C.; Kots, P. A.; Wang, C.; Hinton, Z. R.; Quinn, C. M.; Epps, T. H.; Korley, L. T. J.; Vlachos, D. G. Single pot catalyst strategy to branched products via adhesive isomerization and hydrocracking of polyethylene over platinum tungstated zirconia. *Appl. Catal., B* **2021**, *299*, 13.

(52) Sun, M.; Zhu, L.; Liu, W.; Zhao, X.; Zhang, Y.; Luo, H.; Miao, G.; Li, S.; Yin, S.; Kong, L. Efficient upgrading of polyolefin plastics into C5–C12 gasoline alkanes over a Pt/W/Beta catalyst. *Sustain. Energy Fuels* **2022**.

(53) Utami, M.; Wijaya, K.; Trisunaryanti, W. Pt-promoted sulfated zirconia as catalyst for hydrocracking of LDPE plastic waste into liquid fuels. *Mater. Chem. Phys.* **2018**, *213*, 548-555.

(54) Cecchin, G.; Morini, G.; Piemontesi, F. Ziegler-Natta Catalysts. In *Kirk-Othmer Encyclopedia of Chemical Technology*.

(55) Arlman, E. J. Ziegler-Natta catalysis II. Surface structure of layer-lattice transition metal chlorides. *J. Catal.* **1964**, *3* (1), 89-98.

(56) Burwell, R. L.; Pearson, R. G. The Principle of Microscopic Reversibility. *J. Phys. Chem.* **1966**, *70* (1), 300-302.

(57) Corker, J.; Lefebvre, F.; Lécuyer, C.; Dufaud, V.; Quignard, F.; Choplin, A.; Evans, J.; Basset, J.-M. Catalytic Cleavage of the C-H and C-C Bonds of Alkanes by Surface Organometallic Chemistry: An EXAFS and IR Characterization of a Zr-H Catalyst. *Science* **1996**, *271* (5251), 966-969.

(58) Sinfelt, J. H. Specificity in Catalytic Hydrogenolysis by Metals. In *Advances in Catalysis*, Eley, D. D., Pines, H., Weisz, P. B. Eds.; Vol. 23; Academic Press, 1973; pp 91-119.

(59) Kots, P. A.; Liu, S.; Vance, B. C.; Wang, C.; Sheehan, J. D.; Vlachos, D. G. Polypropylene Plastic Waste Conversion to Lubricants over Ru/TiO2 Catalysts. *ACS Catal.* **2021**, *11* (13), 8104-8115.

(60) Rorrer, J. E.; Troyano-Valls, C.; Beckham, G. T.; Román-Leshkov, Y. Hydrogenolysis of Polypropylene and Mixed Polyolefin Plastic Waste over Ru/C to Produce Liquid Alkanes. *ACS Sustainable Chem. Eng.* **2021**, *9* (35), 11661-11666.

(61) Lapuerta, M.; Hernández, J. J.; Sarathy, S. M. Effects of methyl substitution on the auto-ignition of C16 alkanes. *Combust. Flame* **2016**, *164*, 259-269.

(62) Wang, C.; Xie, T.; Kots, P. A.; Vance, B. C.; Yu, K.; Kumar, P.; Fu, J.; Liu, S.; Tsilomelekis, G.; Stach, E. A.; et al. Polyethylene Hydrogenolysis at Mild Conditions over Ruthenium on Tungstated Zirconia. *JACS Au* **2021**, *1* (9), 1422-1434.

(63) Oya, S.-i.; Kanno, D.; Watanabe, H.; Tamura, M.; Nakagawa, Y.; Tomishige, K. Catalytic Production of Branched Small Alkanes from Biohydrocarbons. *ChemSusChem* **2015**, *8* (15), 2472-2475.

(64) Jing, Y. X.; Wang, Y. Q.; Furukawa, S. Y.; Xia, J.; Sun, C. Y.; Hulsey, M. J.; Wang, H. F.; Guo, Y.; Liu, X. H.; Yan, N. Towards the Circular Economy: Converting Aromatic Plastic Waste Back to Arenes over a Ru/Nb2O5 Catalyst. *Angew. Chem. Int., Ed. Engl.* **2021**, *60* (10), 5527-5535.

(65) Dong, L.; Lin, L.; Han, X.; Si, X.; Liu, X.; Guo, Y.; Lu, F.; Rudić, S.; Parker, S. F.; Yang, S.; et al. Breaking the Limit of Lignin Monomer Production via Cleavage of Interunit Carbon–Carbon Linkages. *Chem* **2019**, *5* (6), 1521-1536.

(66) Barnard, E.; Rubio Arias, J. J.; Thielemans, W. Chemolytic depolymerisation of PET: a review. *Green Chem.* **2021**, *23* (11), 3765-3789.

(67) Milstein, D. Discovery of Environmentally Benign Catalytic Reactions of Alcohols Catalyzed by Pyridine-Based Pincer Ru Complexes, Based on Metal–Ligand Cooperation. *Top. Catal.* **2010**, *53* (13), 915-923.

(68) Balaraman, E.; Fogler, E.; Milstein, D. Efficient hydrogenation of biomass-derived cyclic di-esters to 1,2-diols. *Chem. Commun.* **2012**, *48* (8), 1111-1113.

(69) Krall, E. M.; Klein, T. W.; Andersen, R. J.; Nett, A. J.; Glasgow, R. W.; Reader, D. S.; Dauphinais, B. C.; Mc Ilrath, S. P.; Fischer, A. A.; Carney, M. J.; et al. Controlled hydrogenative depolymerization of polyesters and polycarbonates catalyzed by ruthenium(ii) PNN pincer complexes. *Chem. Commun.* **2014**, *50* (38), 4884-4887.

(70) Papageorgiou, D. G.; Roumeli, E.; Chrissafis, K.; Lioutas, C.; Triantafyllidis, K.; Bikiaris, D.; Boccaccini, A. R. Thermal degradation kinetics and decomposition mechanism of PBSu nanocomposites with silica-nanotubes and strontium hydroxyapatite nanorods. *Phys. Chem. Chem. Phys.* **2014**, *16* (10), 4830-4842, 10.1039/C3CP55103B.

(71) Zhang, H.; Kang, S.; Fu, J.; He, Y.; Huang, X.; Chang, J.; Xu, Y. Valorization of poly(butylene succinate) to tetrahydrofuran via one-pot catalytic hydrogenolysis. *React. Chem. Eng.* **2021**, *6* (3), 465-470.

(72) *Critical mineral resources of the United States—Economic and environmental geology and prospects for future supply*; Reston, VA, 2017. http://pubs.er.usgs.gov/publication/pp1802DOI: 10.3133/pp1802.

(73) Emsley, J. *Nature's building blocks : an A-Z guide to the elements*; Oxford University Press, 2003.

(74) Vance, B. C.; Kots, P. A.; Wang, C.; Granite, J. E.; Vlachos, D. G. Ni/SiO2 catalysts for polyolefin deconstruction via the divergent hydrogenolysis mechanism. *Appl. Catal., B* **2023**, *322*, 122138.

(75) Zichittella, G.; Ebrahim, A. M.; Zhu, J.; Brenner, A. E.; Drake, G.; Beckham, G. T.; Bare, S. R.; Rorrer, J. E.; Román-Leshkov, Y. Hydrogenolysis of Polyethylene and Polypropylene into Propane over Cobalt-Based Catalysts. *JACS Au* **2022**, *2* (10), 2259-2268.

(76) Nakaji, Y.; Nakagawa, Y.; Tamura, M.; Tomishige, K. Regioselective hydrogenolysis of alga-derived squalane over silica-supported ruthenium-vanadium catalyst. *Fuel Process. Technol.* **2018**, *176*, 249-257.

(77) Kots, P. A.; Xie, T.; Vance, B. C.; Quinn, C. M.; de Mello, M. D.; Boscoboinik, J. A.; Wang, C.; Kumar, P.; Stach, E. A.; Marinkovic, N. S.; et al. Electronic modulation of metal-support interactions improves polypropylene hydrogenolysis over ruthenium catalysts. *Nat. Commun.* **2022**, *13* (1), 5186.

(78) Chen, L.; Zhu, Y.; Meyer, L. C.; Hale, L. V.; Le, T. T.; Karkamkar, A.; Lercher, J. A.; Gutiérrez, O. Y.; Szanyi, J. Effect of reaction conditions on the hydrogenolysis of polypropylene and polyethylene into gas and liquid alkanes. *React. Chem. Eng.* **2022**, *7* (4), 844-854.

(79) Rorrer, J. E.; Ebrahim, A. M.; Questell-Santiago, Y.; Zhu, J.; Troyano-Valls, C.; Asundi, A. S.; Brenner, A. E.; Bare, S. R.; Tassone, C. J.; Beckham, G. T.; et al. Role of Bifunctional Ru/Acid Catalysts in the Selective Hydrocracking of Polyethylene and Polypropylene Waste to Liquid Hydrocarbons. *ACS Catal.* **2022**, 13969-13979.

(80) Tamura, M.; Miyaoka, S.; Nakaji, Y.; Tanji, M.; Kumagai, S.; Nakagawa, Y.; Yoshioka, T.; Tomishige, K. Structure-activity relationship in hydrogenolysis of polyolefins over Ru/support catalysts. *Appl. Catal., B* **2022**, *318*, 121870.

(81) Wang, C.; Yu, K.; Sheludko, B.; Xie, T.; Kots, P. A.; Vance, B. C.; Kumar, P.; Stach, E. A.; Zheng, W.; Vlachos, D. G. A General Strategy and a Consolidated Mechanism for Low-methane Hydrogenolysis of Polyethylene over Ruthenium. *Appl. Catal., B* **2022**, 121899.

(82) Khemthong, P.; Klysubun, W.; Prayoonpokarach, S.; Roessner, F.; Wittayakun, J. Comparison between cobalt and cobalt–platinum supported on zeolite NaY: Cobalt reducibility and their catalytic performance for butane hydrogenolysis. *Ind. Eng. Chem.* **2010**, *16* (4), 531-538.

(83) Lomot, D.; Juszczyk, W.; Karpinski, Z.; Larsson, R. Hydrogenolysis of ethane on silica-supported cobalt catalysts. *J. Mol. Catal. A: Chem.* **2002**, *186* (1), 163-172.

(84) Peng, X.; Cheng, K.; Kang, J.; Gu, B.; Yu, X.; Zhang, Q.; Wang, Y. Impact of Hydrogenolysis on the Selectivity of the Fischer–Tropsch Synthesis: Diesel Fuel Production over Mesoporous Zeolite-Y-Supported Cobalt Nanoparticles. *Angew. Chem. Int., Ed. Engl.* **2015**, *54* (15), 4553-4556.

(85) Collins, C. D. Implementing Phytoremediation of Petroleum Hydrocarbons. In *Phytoremediation: Methods and Reviews*, Willey, N. Ed.; Humana Press, 2007; pp 99-108.

(86) Sam, S. T.; Nuradibah, M. A.; Ismail, H.; Noriman, N. Z.; Ragunathan, S. Recent Advances in Polyolefins/Natural Polymer Blends Used for Packaging Application. *Polym. Plast. Technol. Eng.* **2014**, *53* (6), 631-644.

(87) Borkar, S. S.; Helmer, R.; Mahnaz, F.; Majzoub, W.; Mahmoud, W.; Al-Rawashdeh, M. m.; Shetty, M. Enabling resource circularity through thermo-catalytic and solvent-based conversion of waste plastics. *Chem Catal.* **2022**, *2* (12), 3320-3356.

APPENDIX

Table A.1. Effect of stirring rate on PE hydrogenolysis. Reaction conditions: 275 °C, 30 bar initial H_2, 4 h, 0-600 RPM, 2.0 g PE, and 0.1 g Co/SiO_2.

RPM	0	100	200	300	400	600
Gas Yield	5.44%	3.26%	8.12%	5.27%	7.16%	6.22%
Liquid Yield	5.07%	10.91%	25.06%	9.99%	23.42%	14.52%
Waxes	14.78%	7.78%	1.01%	5.80%	5.31%	4.81%
Solid Residue	74.71%	78.05%	65.80%	78.94%	64.11%	74.44%

Table A.2. Gas phase FID retention times and relative response factors

Peak	Name	C_n	RT (min)	RRF
1	Methane	1	8.59	1.000000
2	Ethane	2	10.157	0.895405
3	Propane	3	15.228	0.865238
4	Butane	4	23.619	0.850905
5	Pentane	5	31.227	0.842530

Table A.3. Liquid phase FID retention times and relative response factors

Peak	Name	C_n	RT (min)	RRF
1	n-pentane	5	2.048	1.028432
2	n-hexane	6	2.3	1.021728
3	EtOAc - Solvent		2.4	
4	Benzene - Ext. Standard		2.648	
5	n-heptane	7	2.85	1.021728
6	n-octane	8	3.755	1.016993
7	n-nonane	9	4.987	1.013470
8	n-decane	10	6.391	1.010747
9	n-undecane	11	7.829	1.008579
10	n-dodecane	12	9.232	1.006813
11	n-tridecane	13	10.571	1.005345
12	n-tetradecane	14	11.841	1.004106
13	n-pentadecane	15	13.046	1.003047
14	n-hexadecane	16	14.19	1.002131
15	n-heptadecane	17	15.277	1.001331
16	n-octadecane	18	16.313	1.000626
17	n-nonadecane	19	17.3	0.999441
18	n-eicosane	20	18.245	0.998938
19	n-heneicosane	21	19.149	0.998483

Table A.3. continued

Peak	Name	C_n	RT (min)	RRF
20	n-docosane	22	20.016	0.998070
21	n-tricosane	23	20.85	0.997694
22	n-tetracosane	24	21.651	0.997349
23	n-pentacosane	25	22.423	0.997032
24	n-hexacosane	26	23.166	0.996739
25	n-heptacosane	27	23.885	0.996468
26	n-octacosane	28	24.624	0.996217
27	n-nonacosane	29	25.472	0.995983
28	n-triconntane	30	26.469	0.995983
29	n-C_{30+}	30+	27.652+	0.995765

Table A.4. PE hydrogenolysis temperature series fractional yields and mass balance. Reaction conditions: 200-300 °C, 30 bar initial H_2, 4 h, 200 RPM, 1.0 g PE, and 0.1 g Co/SiO_2.

Hydrogenolysis products		Yield (% C-mol)				
Fraction	C_n	200 °C	225 °C	250 °C	275 °C	300 °C
Methane	1	0.06%	0.91%	4.41%	6.35%	33.42%
Light gases	2-5	0.15%	0.16%	1.26%	1.78%	12.20%
Gasoline	5-12	6.42%	0.28%	2.04%	3.71%	23.22%
Jet fuels	13-15	0.00%	0.06%	0.96%	2.11%	4.52%
Diesel	16-21	0.14%	0.30%	2.01%	4.63%	8.29%
Motor Oil	22-30	0.69%	0.54%	2.20%	6.49%	4.24%
Lubricants	30+	1.89%	0.41%	1.95%	8.37%	1.58%
Mass balance						
Gas Yield		0.21%	1.08%	5.68%	8.12%	45.62%
Liquid Yield		9.14%	1.57%	9.00%	25.06%	40.62%
Solid Residue		90.81%	86.65%	64.41%	65.80%	0.00%
Total Captured		100.16%	89.29%	79.09%	98.99%	86.24%
Liner Mass Balance		106.55%	105.18%	94.42%	101.52%	96.81%

Table A.5. PE hydrogenolysis pressure series fractional yields and mass balance. Reaction conditions: 275 °C, 20-40 bar initial H_2, 4 h, 200 RPM, 1.0 g PE, and 0.1 g Co/SiO_2.

Hydrogenolysis products		Yield (% C-mol)		
Fraction	C_n	20 bar	30 bar	40 bar
Methane	1	9.69%	6.35%	36.75%
Light gases	2-5	1.37%	1.78%	11.41%
Gasoline	5-12	4.92%	3.71%	12.60%
Jet fuels	13-15	2.41%	2.11%	2.89%
Diesel	16-21	5.69%	4.63%	6.75%
Motor Oil	22-30	7.65%	6.49%	4.39%
Lubricants	30+	10.14%	8.37%	1.60%
Mass balance				
Gas Yield		11.06%	8.12%	48.16%
Liquid Yield		30.62%	25.06%	26.74%
Solid Residue		56.93%	65.80%	0.57%
Total Captured		98.61%	98.99%	75.46%
Liner Mass Balance		94.47%	101.52%	86.94%

Table A.6. PE hydrogenolysis time series fractional yields and mass balance. Reaction conditions: 275 °C, 30 bar initial H_2, 2 – 36 h, 200 RPM, 1.0 g PE, and 0.1 g Co/SiO_2.

Hydrogenolysis products		Yield (% C-mol)				
Fraction	C_n	2 h	4 h	8 h	16 h	36 h
Methane	1	5.10%	6.35%	16.66%	29.56%	89.46%
Light gases	2-5	1.84%	1.78%	2.86%	5.47%	0.00%
Gasoline	5-12	4.37%	3.71%	9.92%	6.07%	0.00%
Jet fuels	13-15	2.30%	2.11%	6.49%	1.31%	0.00%
Diesel	16-21	5.12%	4.63%	13.42%	7.47%	0.07%
Motor Oil	22-30	6.63%	6.49%	18.18%	16.16%	1.70%
Lubricants	30+	6.05%	8.37%	10.55%	5.34%	0.17%
Mass balance						
Gas Yield		6.94%	8.12%	19.52%	35.03%	89.46%
Liquid Yield		24.19%	25.06%	58.18%	35.40%	1.94%
Solid Residue		70.29%	65.80%	27.68%	24.20%	-0.74%
Total Captured		101.41%	98.99%	105.37%	94.64%	90.65%
Liner Mass Balance		100.81%	101.52%	99.92%	99.09%	102.52%

Table A.7. PE hydrogenolysis recycle series fractional yields and mass balance. Reaction conditions: 300 °C, 30 bar initial H_2, 4 h, 200 RPM, 1.0 g PE, 0.1 (initially, followed by recovered mass) g Co/SiO_2.

Hydrogenolysis products		Yield (% C-mol)			
Fraction	C_n	0	1	2	3
Methane	1	77.95%	10.89%	7.66%	5.58%
Light gases	2-5	4.01%	7.27%	8.89%	10.15%
Gasoline	5-12	0.35%	25.00%	28.34%	28.66%
Jet fuels	13-15	0.09%	9.15%	9.80%	9.06%
Diesel	16-21	2.39%	12.86%	12.82%	11.34%
Motor Oil	22-30	3.74%	6.10%	7.39%	6.85%
Lubricants	30+	0.77%	1.21%	1.05%	3.25%
Gas Yield		81.96%	18.16%	16.55%	15.73%
Liquid Yield		7.34%	53.56%	58.51%	58.21%
Solid Residue		0.38%	-0.51%	0.23%	0.43%
Total Captured		89.68%	71.22%	75.29%	74.37%
Liner Mass Balance		100.50%	84.36%	78.39%	74.82%

Table A.8. PE hydrogenolysis regeneration series fractional yields and mass balance. Reaction conditions: 300 °C, 30 bar initial H_2, 4 h, 200 RPM, 1.0 g (Run 0) and ~0.55 g (Run 1) PE, 0.1 g (Run 0) and ~0.055 g (Run 1) Co/SiO_2.

Hydrogenolysis Products		Yield (% C-mol)	
Fraction	C_n	Run 0	Run 1
Methane	1	36.23%	30.91%
Light gases	2-5	13.77%	14.84%
Gasoline	5-12	11.60%	6.59%
Jet fuels	13-15	2.70%	1.64%
Diesel	16-21	5.59%	6.16%
Motor Oil	22-30	3.31%	6.48%
Lubricants	30+	0.22%	0.73%
Mass balance			
Gas Yield		50.00%	45.75%
Liquid Yield		22.01%	19.60%
Solid Residue		-0.31%	2.96%
Total Captured		71.70%	68.30%
Liner Mass Balance		88.79%	91.84%

Table A.9. End-of-use plastic hydrogenolysis series fractional yields and mass balance. Reaction conditions: 275 °C, 30 bar initial H_2, 8 h, 200 RPM, 1.0 g substrate, and 0.1 g Co/SiO_2.

Hydrogenolysis Products		Yield (% C-mol)			
Fraction	C_n	HDPE jug	LDPE bag	LDPE bottle	PP cups
Methane	1	46.44%	40.16%	51.00%	3.81%
Light gases	2-5	7.75%	7.54%	9.96%	2.47%
Gasoline	5-12	6.74%	4.89%	3.76%	8.17%
Jet fuels	13-15	2.10%	1.24%	0.91%	3.81%
Diesel	16-21	6.82%	3.94%	5.19%	3.15%
Motor Oil	22-30	11.58%	5.37%	8.90%	2.39%
Lubricants	30+	1.28%	3.68%	1.41%	15.99%
Mass balance					
Gas Yield		54.18%	47.70%	60.96%	6.28%
Liquid Yield		27.31%	18.02%	18.86%	32.62%
Solid Residue		8.57%	25.81%	8.43%	66.59%
Total Captured		90.06%	91.53%	88.25%	105.49%
Liner Mass Balance		90.02%	94.08%	94.80%	91.66%